



1 **Air quality impacts of COVID-19 lockdown measures detected**
2 **from space using high spatial resolution observations of multiple**
3 **trace gases from Sentinel-5P/TROPOMI**

4 Pieterneel F. Levelt^{1,2}, Deborah C. Stein Zweers¹, Ilse Aben³, Maite Bauwens⁴, Tobias Borsdorff³,
5 Isabelle De Smedt⁴, Henk J. Eskes¹, Christophe Lerot⁴, Diego G. Loyola⁵, Fabian Romahn⁵,
6 Trissevgeni Stavrakou⁴, Nicolas Theys⁴, Michel Van Roozendael⁴, J. Pepijn Veefkind^{1,2}, Tijl
7 Verhoelst⁴

8 ¹Royal Netherlands Meteorological Institute (KNMI), De Bilt, 3731GA, The Netherlands

9 ²University of Technology Delft (TU Delft), Delft, 2628 CN, the Netherlands

10 ³Netherlands Institute for Space Research (SRON), Utrecht, 3584 CA, The Netherlands

11 ⁴Royal Belgian Institute for Space Aeronomy (BIRA-IASB), Brussels, 1180, Belgium

12 ⁵German Aerospace Centre (DLR), Oberpfaffenhofen, Wessling, 82234, Germany

13 *Correspondence to:* Deborah C. Stein Zweers (stein@knmi.nl)

14 **Abstract.** The aim of this paper is two-fold: to provide guidance on how to best interpret TROPOMI trace gas
15 retrievals and to highlight how TROPOMI trace gas data can be used to understand event-based impacts on air quality
16 from regional to city-scales around the globe. For this study, we present the observed changes in the atmospheric
17 column amounts of five trace gases (NO₂, SO₂, CO, HCHO and CHOCHO) detected by the Sentinel-5P TROPOMI
18 instrument, driven by reductions of anthropogenic emissions due to COVID-19 lockdown measures in 2020. We report
19 clear COVID-19-related decreases in NO₂ concentrations on all continents. For megacities, reductions in column
20 amounts of tropospheric NO₂ range between 14% and 63%. For China and India supported by NO₂ observations,
21 where the primary source of anthropogenic SO₂ is coal-fired power generation, we were able to detect sector-specific
22 emission changes using the SO₂ data. For HCHO and CHOCHO, we consistently observe anthropogenic changes in
23 two-week averaged column amounts over China and India during the early phases of the lockdown periods. That these
24 variations over such a short time scale are detectable from space, is due to the high resolution and improved sensitivity
25 of the TROPOMI instrument. For CO, we observe a small reduction over China which is in concert with the other
26 trace gas reductions observed during lockdown, however large, interannual differences prevent firm conclusions from
27 being drawn. The joint analysis of COVID-19 lockdown-driven reductions in satellite observed trace gas column
28 amounts, using the latest operational and scientific retrieval techniques for five species concomitantly is
29 unprecedented. However, the meteorologically and seasonally driven variability of the five trace gases does not allow
30 for drawing fully quantitative conclusions on the reduction of anthropogenic emissions based on TROPOMI
31 observations alone. We anticipate that in future, the combined use of inverse modelling techniques with the high
32 spatial resolution data from S5P/TROPOMI for all observed trace gases presented here, will yield a significantly
33 improved sector-specific, space-based analysis of the impact of COVID-19 lockdown measures as compared to other
34 existing satellite observations. Such analyses will further enhance the scientific impact and societal relevance of the
35 TROPOMI mission.

36



37 **Key words:** Air quality, Trace gases, Sentinel-5P, TROPOMI, COVID-19, emissions

38 1 Introduction

39 In an effort to limit the transmission of the SARS-CoV-2 virus responsible for the Coronavirus disease 2019 (hereafter
40 referred as COVID-19), drastic lockdown measures were implemented around the globe in the first half of 2020. These
41 policies led to dramatic reductions in human activity, especially in the transport and industrial sectors, resulting in
42 large decreases in the concentration of air pollutants (Bauwens et al., 2020; Shi and Brasseur, 2020; Forster et al.,
43 2020; Diamond and Wood, 2020; Kroll et al., 2020; Le Quéré et al., 2020; Guevara et al., 2021; Gkatzelis et al., 2021).
44 These changes were observed over China as early as February 2020 (Bauwens et al., 2020; Liu et al., 2020; Zhang, Z.
45 et al., 2020; Zhao, N. et al., 2020) and were detected later in many other countries as similar lockdown measures were
46 adopted (Bauwens et al., 2020; Broomandi et al., 2020; Collivignarelli et al., 2020; Lee et al., 2020; Gkatzelis et al.,
47 2021).

48 The Tropospheric Monitoring Instrument (TROPOMI; Veefkind et al., 2012; Ludewig et al., 2020) on board the
49 European Copernicus Sentinel-5 Precursor (S5P) satellite, launched on 13 October 2017, is specifically designed for
50 tropospheric monitoring on the global scale and has a daily revisit time. Compared to its predecessor OMI,
51 TROPOMI's highest spatial resolution ($3.5 \times 5.5 \text{ km}^2$) is about 16 times better and its signal-to-noise ratio per ground
52 pixel is substantially higher. This results in a spectacular improvement in measurement sensitivity for relevant air
53 quality products, including NO_2 , SO_2 , HCHO, and CHOCHO, thus enabling the study of rapid emission changes for
54 even smaller sources as compared to previous instruments. For CO measurements, the daily global coverage of
55 TROPOMI at a resolution of $7 \times 5.5 \text{ km}^2$ represents a huge improvement to its predecessor SCIAMACHY
56 (Bovensmann et al., 1999; Borsdorff et al., 2016; Borsdorff et al., 2017) with a spatial resolution of $120 \times 30 \text{ km}^2$.

57 The observations from TROPOMI thus provide a unique opportunity to observe the magnitude and timing of the
58 changes in tropospheric trace gas constituents, resulting from unprecedented COVID-19 lockdown measures. The
59 initial TROPOMI observations of dramatic reductions in NO_2 concentrations over regions with strictly enforced
60 lockdowns, over China in particular, triggered a high level of interest worldwide, and initiated a large number of
61 studies, mainly aimed at regional scales and largely focused on NO_2 . However, the unparalleled capacity of TROPOMI
62 to provide relevant information on COVID-19 driven emission reductions based on multiple species measurements
63 has not been exploited yet. The objective of this work is to investigate the COVID-19 driven changes in the
64 concentration of five trace gases (NO_2 , SO_2 , CO, HCHO, and CHOCHO) from the global level down to individual
65 cities using state-of-the-art TROPOMI operational and scientific data products. More specifically, we aim to

- 66 1. Expand the analysis of tropospheric NO_2 to all continents.

67 A large body of studies investigated the impact of the COVID-19 lockdowns on NO_2 concentrations (e.g. Bauwens et
68 al., 2020; Baldasano, 2020; Huang et al., 2020), at regional and continental scale. Here, we analyze the time series of
69 NO_2 measurements from a single satellite instrument for globally distributed locations on regional to city scales. In
70 doing so, we further demonstrate the unique capabilities of how the TROPOMI instrument can be used to consistently
71 track changes in air quality and anthropogenic emissions across the globe.

72



73 2. Explore the high spatial resolution and simultaneous TROPOMI observations of NO₂, SO₂, CO, HCHO, and
74 CHOCHO.

75 While all of these gases have significant anthropogenic sources, they differ in their relative contribution to the energy,
76 industry, and transport sector emissions, and each sector exhibits a different response to COVID-19 lockdown
77 measures. Therefore, the combination of several TROPOMI trace gas products contains additional information on
78 sector-specific emissions and COVID-19 lockdown-induced changes in atmospheric composition. We show that
79 meaningful trends and source detection can be obtained by using the unprecedentedly high spatial resolution of
80 TROPOMI data and by averaging that data over relatively short time periods. Although this is in large part the result
81 of the improved sensitivity of the instrument, we also introduce new developments in trace gas retrieval techniques
82 and ad-hoc corrections to enhance the sensitivity of the TROPOMI datasets to even smaller emissions and smaller
83 changes in emissions. In order to achieve these goals, we discuss the strengths and limitations of each of the retrievals
84 for tracking global to city-scale changes.

85 In the next section, the TROPOMI data will first be described in general terms, followed by a description per species
86 to address the retrieval methods, as well as a description of how we handle each data product in this study. The goal
87 of this methods and data section is not only to explain how this study was conducted but also to provide guidance to
88 data users on how to best interpret and analyze TROPOMI trace gas data not only for lockdown-driven emission
89 changes but also for other event-driven changes. This will be followed by a section describing the impacts of COVID-
90 19 lockdown measures on all continents, using TROPOMI NO₂ data. The next two sections will describe the effect of
91 the lockdown measures on a regional scale by examining NO₂, SO₂, CO, HCHO, and CHOCHO for China and India.
92 The last section will feature an outlook of future applications for this type of analysis followed by conclusions.

93 **2 Methods and Data**

94 In this work, our analysis is primarily based on TROPOMI data for regional lockdown periods in 2020 as compared
95 to the same periods in 2019 and will be presented in the broader context of the TROPOMI operational data record,
96 which started on 30 April 2018. We make use of observations from the TROPOMI instrument on board S5P which is
97 a push-broom imaging spectrometer (Veefkind et al., 2012) measuring in the ultraviolet (UV), visible (VIS), near-
98 infrared (NIR), and shortwave infrared (SWIR) spectral bands selected to cover absorption regions for clouds and a
99 large number of trace atmospheric constituents. Using the spectral radiance measurements from TROPOMI,
100 atmospheric concentrations of different gases are retrieved as well as cloud and aerosol properties. For this work, we
101 use the following TROPOMI data products: NO₂, SO₂, CO, HCHO and CHOCHO as summarized in Table 1. We did
102 not include the following TROPOMI data products: tropospheric ozone columns, due to the tropics-only spatial
103 coverage; methane, due to an even longer atmospheric lifetime than CO where its sources were not as impacted by
104 lockdown measures; and aerosol index, designed to highlight long-range transported and/or elevated plumes of smoke,
105 dust, and/or ash and which is not a quantitative measure of aerosol amount nor sensitive to near-surface emissions.

106 The S5P satellite flies in a Sun-synchronous orbit, with a local overpass time of 13:30. TROPOMI has a 2600 km
107 wide swath, providing near-daily global coverage. The spatial sampling of TROPOMI varies over the spectral bands.
108 The nadir sampling at the start of the operational period on 30 April 2018 was approximately 3.5 x 7 km² (across- x



109 along-track) for the ultraviolet and visible bands, and $7 \times 7 \text{ km}^2$ in the shortwave infrared band. On 6 August 2019,
110 after implementation of a modified co-adding scheme, the sampling for these bands was improved to $3.5 \times 5.5 \text{ km}^2$
111 and $7 \times 5.5 \text{ km}^2$, respectively.

112 TROPOMI observations are being widely used within and beyond the scientific community and so it is crucial to
113 provide information on how these observations can best be used, interpreted, and analyzed. The COVID-19 lockdown
114 periods provide a unique use-case for the TROPOMI lead algorithm developers to highlight important differences in
115 the individual atmospheric lifetime and detectability of each trace gas and show how these characteristics are key to
116 the interpretation of the concomitant observations. It is not sufficient, for example, to illustrate lockdown-driven
117 changes in emissions simply by selecting a single day or week of TROPOMI column data for a given region as
118 measured during a lockdown period to the same day or week from year(s) prior (Braaten et al., 2020). We go further
119 to address the importance of delineating meteorological and seasonal variability from lockdown-driven changes in
120 emissions.

121 Therefore, we start this methods and data section with a general overview of considerations for the data user to take
122 into account for analyses aimed at the quantification of changes in the emission of these trace gases. Next, in dedicated
123 subsections, we provide a summary of the most relevant documentation and retrieval methods employed for each trace
124 gas (see Table A1). Even though each retrieval is based on the analysis of the amount of trace gas specific absorption
125 in measured radiance spectra, methods differ significantly per species.

126 2.1 Understanding and Interpreting TROPOMI trace gas retrievals

127 For this paper we will focus on TROPOMI trace gas retrievals for NO_2 , SO_2 , CO, HCHO, and CHOCHO (See Table
128 1). To understand and interpret the TROPOMI measurements of these trace gas species and how they vary with respect
129 to COVID-19 lockdown measures, it is necessary to consider their sources, variability through the atmospheric
130 column, and their atmospheric lifetimes. Although the mechanisms for the emission of each gas are different, there
131 are several common anthropogenic emission sources, most notably from transportation and industry, as listed in Table
132 1 which were significantly impacted by lockdown measures.

133

134 **Table 1: Summary of the retrieval spectral range, atmospheric lifetime, and primary emission sources, for each trace gas**
135 **addressed in this study.**

Trace Gas (retrieval reference)	Spectral Range	Typical lifetime	Primary emission sources
NO_2 (van Geffen et al., 2019)	405-465 nm	2 to 12 hours	- Transportation - Industry - Power generation - Biomass burning
SO_2 (Theys et al., 2021)	310.5-326 nm	6 hours to several days	- Power generation - Industry - Transportation - Volcanoes ¹



CO (Landgraf et al., 2016)	2324–2338 nm	Weeks to a month	- Power generation - Industry - Transportation - Residential cooking and heating - Biomass burning - Oxidation of biogenic hydrocarbons - Methane Oxidation
HCHO (De Smedt et al., 2018)	328.5–359 nm	Several hours (lifetime of NMVOC precursors up to several days)	Primary and secondary product (NMVOC precursors) from: - Biogenic emissions - Biomass burning - Industry - Transportation
CHOCHO (Lerot et al., 2010, 2020)	435–460 nm	2 to 3 hours	Primary and secondary product (NMVOC precursors) from: - Biogenic emissions - Biomass burning - Transportation - Industry

136 ¹Volcanic emissions are not significant for this work.

137

138 A brief evaluation of how the sources of these trace gases were or were not affected by lockdown-driven changes
139 lends insight into expected changes. In general, primary production trace gases, like NO₂ and SO₂ with relatively short
140 atmospheric lifetimes exhibit emission changes most clearly and rapidly. Although NO₂ and SO₂ are both important
141 primary production anthropogenic pollutants, their sectoral sources are different. For instance, the impact of lockdown
142 on the transportation sector is expected to have a bigger impact on NO₂ than SO₂, since this sector is responsible for
143 about 30% of the global NO_x emissions and only 1% of the global SO₂ emissions, according to the CAMS-ANT
144 inventory (Granier et al., 2019). On the other hand, SO₂ emissions are more likely to be impacted by possible changes
145 in power generation, since this sector accounts for 52% of the global SO₂ emissions and only 30% of the global NO_x
146 emission (Granier et al., 2019).

147 For CO, secondary production by methane oxidation and the oxidation of (biogenic) hydrocarbons accounts for at
148 least 60% of the total atmospheric CO, followed by contributions from biomass burning and fossil fuel use (Müller et
149 al., 2018; Holloway et al., 2000). Anthropogenic CO emissions originate from the industry, transportation, and
150 residential sectors and account for about 30% of the global emissions (Granier et al., 2019). Although local impacts
151 of lockdown are likely for locations with strong anthropogenic CO emissions, overall a much smaller lockdown-driven
152 impact is expected for CO based on its longer atmospheric lifetime and smaller contributions from lockdown affected
153 sources.

154 Both HCHO and CHOCHO are short-lived indicators of non-methane volatile organic compound (NMVOC)
155 emissions resulting from biogenic processes, large biomass burning events, and anthropogenic activities (Millet et al.,



156 2008; Fu et al., 2008; Stavrou et al., 2009; Bauwens et al., 2016; Chan Miller et al., 2016). They are mostly produced
157 as secondary products from oxidation of other NMVOCs but are also directly emitted from combustion and industrial
158 processes, although to a lesser extent. In general, the relative production of CHOCHO from such combustion processes
159 and from the oxidation of aromatics, originating mostly from the industrial sector, is higher than for HCHO. Thus, the
160 CHOCHO response to changes in anthropogenic emissions is expected to be stronger (Chan Miller et al., 2016; Cao
161 et al., 2018).

162 It is important to note that the retrievals provide information on the tropospheric or total column amount of these
163 gases, because the spectra contain limited information on their vertical distribution in the atmosphere. TROPOMI
164 observations thus provide a two-dimensional representation of the three-dimensional atmosphere. The vertical profiles
165 of each trace gas vary significantly depending on the injection height of the emissions and atmospheric lifetime (see
166 Table 1). For example, NO_x emissions at the surface result in NO₂ vertical profiles that peak in the near-surface layer
167 (lowest 1-2 km of the troposphere), due to the short lifetime of NO₂. Similarly, SO₂ has a vertical profile which
168 generally peaks in the lower troposphere. CO on the other hand, has a lifetime of weeks to a month (depending on the
169 reaction with the hydroxyl radical) and can be transported over great distances, both horizontally and vertically.
170 Therefore, CO even though it is often co-emitted with NO₂, has a significantly higher background concentration
171 throughout the troposphere as compared to NO₂. HCHO and CHOCHO have lifetimes of a few hours but are generally
172 formed in the atmosphere via secondary production processes, which leads to an intermediate profile shape as
173 compared to NO₂ and CO.

174 In addition to vertical profiles that vary per trace gas species, the vertical sensitivity of the TROPOMI measurements
175 also varies per species. For the trace gases retrieved in the UV and VIS ranges, the sensitivity decreases towards the
176 surface so that the accuracy of the retrieved column depends on a well-characterized a priori knowledge of the vertical
177 distribution. Due to scattering, the near-surface sensitivity is lower in the UV (SO₂, HCHO) than in the VIS (NO₂ and
178 CHOCHO). In the SWIR range, the vertical sensitivity is more constant. As part of the retrieval process, a priori
179 vertical profiles of each trace gas are scaled to match the measured tropospheric column. An uncertainty in the
180 retrieved column amount or vertical column density (VCD) is associated with inherent differences between the true
181 and a priori vertical profiles. However, the averaging kernels, which are reported in the data products, can be used to
182 replace the a priori profiles with custom profiles (e.g. Eskes and Boersma, 2003; Eskes et al., 2020) thereby reducing
183 the corresponding uncertainty. In this study, we mostly focus on relative changes in VCDs and use standard a priori
184 profiles for each data product. Therefore, the uncertainty related to the vertical profile is rather small (as detailed in
185 Sect. 2.2 through 2.6). Another contribution to this error is the use of partly cloudy scenes by each retrieval which
186 increases the amount of data available but does change the vertical sensitivity. The cloud fraction threshold for each
187 trace gas is described in Sect. 2.2 through 2.6. In future studies, the averaging kernels could be used for inversion
188 modelling of emissions thus eliminating this error completely.

189 TROPOMI observes atmospheric concentrations of trace gases averaged over a vertical column, which is not the
190 same as a direct measurement of the (near-surface) emission. The column averaged amount of a given trace gas
191 measured at a certain location depends not only on emission and deposition, but also on atmospheric transport and
192 (photo)chemical reactions. Note that the background concentration is higher for trace gases with a longer atmospheric



193 lifetime. In turn, enhanced background concentrations will increase the relative importance of atmospheric transport
194 versus local emissions. Local NO₂ emissions have a relatively large impact on the measured column amounts, while
195 for CO the contribution of remote sources can in some cases be superimposed on local emissions thus making the
196 interpretation more difficult. To attribute a change in concentration to a corresponding change in local emissions, the
197 effects of meteorology and chemical lifetime must be accounted for as well.

198 While emissions can be estimated from satellite observations using data-driven methods (Beirle et al., 2019, Beirle
199 et al., 2021; Fioletov et al., 2016; Goldberg et al., 2019) or using complex inverse modelling techniques (e.g. Millet
200 et al., 2008; Stavrou et al., 2009; Bauwens et al., 2016; Ding et al., 2020; Miyazaki et al., 2020; Borsdorff et al.,
201 2019; Borsdorff et al., 2020), here we use a more qualitative approach to probe emission changes. First we compare
202 the concentrations in 2020 with those from the same period from earlier years and then carry out additional analysis
203 to separate the lockdown-driven variability from seasonal and meteorological variability taking in account emission
204 changes driven by mechanisms.

205 2.2 Nitrogen dioxide (NO₂)

206 The tropospheric column of nitrogen dioxide (NO₂) is a TROPOMI operational data product (Veeckind et al., 2012;
207 doi.org/10.5270/S5P-s4ljg54). Product versions are listed in the Product Readme File (PRF, Eskes and Eichmann,
208 2019a). The retrieval method is described in detail in the NO₂ Algorithm Theoretical Basis Document (ATBD, van
209 Geffen et al., 2019). The data product and data usage are described in in the NO₂ Product User Manual (PUM, Eskes
210 et al., 2020). The dataset used for most of NO₂ analyses cover the period from 1 January 2018 to 30 May 2020. For
211 Europe, the dataset was extended through 31 August 2020.

212 The retrieval algorithm derives NO₂ information from spectral range 405-465 nm and is largely based on the OMI
213 NO₂ retrieval developments implemented during the EU QA4ECV project (Boersma et al., 2018). The retrieval
214 consists of three steps. The first step is based on the DOAS approach, in which the total slant column of NO₂ is
215 retrieved from the TROPOMI spectra, as discussed in van Geffen et al. (2020). The second step is the estimation of
216 the 3-D stratospheric distribution of NO₂ based on an assimilation of the TROPOMI slant column data of previous
217 days using the chemistry-transport model TM5-MP (Williams et al., 2017) run at 1° x 1°. This assimilation is set up
218 to predominantly make use of measurements over clean areas (e.g. ocean and remote land regions) with limited
219 tropospheric NO₂. The third step is the conversion of the tropospheric slant column (total minus stratosphere) into a
220 tropospheric vertical column by combining radiative transfer calculations with a priori profile shapes from the TM5-
221 MP model. The data product is very comprehensive and provides all the input (such as surface and cloud information)
222 and intermediate products.

223 The tropospheric column is delivered with corresponding averaging kernels and a detailed error estimate. The
224 random error on the slant column is discussed in van Geffen et al. (2020), and is on the order of 0.56x10¹⁵ molec cm⁻²
225 for individual measurements after 6 August 2019 (for pixel size 3.5 x 5.5 km²). This translates to only small random
226 errors in the total columns on the order of 0.2x10¹⁵ molec cm⁻². Uncertainties in the estimate of the local stratospheric
227 column amount is of the same order of magnitude. The uncertainty related to the computation of the air mass factor
228 (AMF) is much more significant for tropospheric columns over polluted areas. The AMF uncertainties are driven by



229 the treatment of surface albedo, clouds, aerosols, and profile shape. Such errors are multiplicative, and are of the order
230 of 20-60% depending on the geographical location, time of day, and season. These uncertainties are modelled for
231 individual observations and are provided in the data product.

232 As for all operational TROPOMI data products, a quality assurance value (qa_value) is provided to filter the data
233 and remove lower quality data where, the recommended threshold value depends on the application. For direct
234 visualization or gridding applications a qa_value greater than 0.75 is recommended. For comparisons with models and
235 data assimilation through the use of the averaging kernels, a relaxed qa_value of greater than 0.5 may be used. In this
236 study we use NO₂ retrievals with a qa_value greater than 0.75. Application of this qa_value threshold corresponds to
237 data with mostly clear-sky conditions (cloud radiance fractions < 0.5) and implies that the data is filtered to remove
238 retrievals which do not meet certain quality criteria as described van Geffen et al. (2019).

239 Several recent papers discuss the validation of the NO₂ product against independent observations (Verhoelst et al.,
240 2021; Tack et al., 2021; Judd et al., 2020; Dimitropoulou et al., 2020; Ialongo et al., 2020). The main findings can be
241 summarized as follows: the stratospheric and slant columns are in good overall agreement with other satellite
242 measurements (van Geffen et al., 2020) and with ground-based observations (Verhoelst et al., 2021). However, the
243 tropospheric column presents a negative bias of the order of 30% with respect to ground-based remote sensing
244 reference observations (Verhoelst et al., 2021; Dimitropoulou et al., 2020), as well as with imaging data from airborne
245 measurements (Judd et al., 2020; Tack et al., 2021). Although the origin of this bias remains unclear and may be due
246 to several causes, validation results indicate that it scales linearly with the retrieved tropospheric column amount
247 (Verhoelst et al., 2021; see Fig. C1). As a result, (COVID-related) relative changes in the NO₂ column, e.g., (2020-
248 2019)/2019, should be largely insensitive to this bias.

249 2.3 Sulphur dioxide (SO₂)

250 Initial analyses were performed using the TROPOMI operational data product for SO₂ (Theys et al., 2017). However,
251 biases present in those data (Fioletov et al., 2020) hamper the detection of the type of small changes in SO₂, typically
252 on the order of -0.1 DU, that are under investigation in this work. Therefore, an alternative retrieval scheme was
253 applied, the so-called COvariance-Based Retrieval Algorithm (COBRA; Theys et al., 2021). In brief, the approach
254 considers a set of SO₂-free spectra in the wavelength range 310.5-326.0 nm (from TROPOMI band 3) to represent the
255 radiance background variability, in the form of a covariance matrix. The latter is updated for each orbit, TROPOMI
256 row, and per latitude band. The covariance matrix is used to determine the SO₂ slant columns from individual spectral
257 measurements using an optimally weighted single parameter retrieval (see Walker et al., 2011). We note that COBRA
258 does not recalculate air mass factors (AMF). These are simply extracted from the operational product to convert SO₂
259 slant columns into vertical columns (VCDs). Compared to the operational DOAS results, COBRA significantly
260 improves the SO₂ VCDs, both in terms of precision and accuracy. Because the approach empirically accounts for all
261 sources of systematic variability in the measured signal, large-scale biases typically observed with the DOAS approach
262 are efficiently removed leading to a large gain in sensitivity (see Fig. C2).

263 In this study, we use SO₂ retrievals under clear-sky conditions (cloud fractions less than 30%) with solar zenith
264 angles lower than 60°, and we eliminate 25 swath edge pixels from each side of the orbit swath (450 pixels wide). The



265 random error in the SO₂ vertical columns is rather small in the range of 0.5-1.0 DU, and can be largely reduced by
266 data averaging. Errors due to spectral interferences are estimated to be very low, about 0.05 DU. Remaining systematic
267 uncertainties are mostly from the auxiliary data used in the AMF calculation, and are in the 30-50% range. The dataset
268 used for this analysis covers the period from May 2018 to June 2020.

269 **2.4 Carbon monoxide (CO)**

270 The total column of carbon monoxide (CO) is a TROPOMI operational data product obtained using TROPOMI 2.3
271 micron measurements (Veeffkind et al., 2012; doi.org/10.5270/S5P-1hkp7rp). Product versions are listed in the Product
272 Readme File (Landgraf et al., 2020). The data product and data usage are described in in the CO Product User Manual
273 (Apituley et al., 2018). This CO retrieval uses the Shortwave Infrared CO retrieval (SICOR) algorithm method and is
274 described in detail in the CO Algorithm Theoretical Basis Document (Landgraf et al., 2018). The algorithm software
275 is based on a scattering forward model and retrieves trace gas columns simultaneously with effective cloud parameters
276 (cloud height, cloud optical thickness) from the SWIR channel to account for cloud contaminated measurements
277 (Landgraf et al., 2016, 2018). The inversion deploys a profile scaling approach by which a vertical CO reference
278 profile is scaled to obtain agreement between the forward simulation and the spectral measurement (Borsdorff et al.,
279 2014). The reference profile is based on a monthly averaged simulation from the global chemical transport model
280 TM5 and thus varies spatially and temporally (Krol et al., 2005). The vertical sensitivity of the retrieval for clear-sky
281 conditions is good throughout the atmosphere while measurements for cloudy conditions have reduced sensitivity
282 under the cloud (Borsdorff et al., 2018).

283 In this study, we use the CO retrieval for measurements under clear-sky and cloudy atmospheric conditions (cloud
284 altitude less than 5000m). This corresponds to filtering the dataset by using the quality assurance values (qa_value
285 greater than 0.5) that are supplied with the data product. CO retrievals under low cloud conditions perform well for
286 unpolluted scenes however can lead to e.g. lower CO values when pollution hot spots are present below the cloud due
287 to optical shielding and scattering (Borsdorff et al., 2018). Consequently, retrievals under cloudy conditions must be
288 considered with care, however they are essential to improve the data coverage especially over the oceans where clear-
289 sky measurements are hampered by the low reflectivity of water in the SWIR spectral range.

290 The CO retrieval skill lies well within the requirements of the TROPOMI mission (Veeffkind et al., 2012) on accuracy
291 (< 15%) and precision (< 10%). This was shown by validation with ground-based FTIR measurements operated by
292 the Total Carbon Column Observing Network (TCCON). TROPOMI CO is biased high compared to TCCON by
293 about 6 ppb with a station to station variability of about 4 ppb (Borsdorff et al., 2018; Lambert et al., 2020). The
294 dataset used for this analysis covers the period from 1 January 2018 to 30 May 2020.

295 **2.5 Formaldehyde (HCHO)**

296 The tropospheric column of formaldehyde (HCHO) is a TROPOMI operational data product (Veeffkind et al., 2012;
297 doi:10.5270/S5P-tjlxfd2). Product versions are listed in the HCHO Product Readme File (De Smedt et al., 2020a).
298 The data product and data usage are described in in the HCHO Product User Manual (PUM, Romahn et al., 2020).
299 The TROPOMI HCHO retrieval algorithm has been fully described in De Smedt et al. (2018) and in the HCHO ATBD



300 (De Smedt et al., 2020b). It is based on the DOAS method, and is directly inherited from the OMI QA4ECV product
301 (<https://doi.org/10.18758/71021031>). The fit of the slant columns is performed in the spectral interval of 328.5-359.0
302 nm. Reference spectra are updated daily using an average of Earth radiances selected in the Equatorial Pacific region.
303 The conversion from total slant to tropospheric vertical columns is performed using a look-up table of vertically
304 resolved air mass factors calculated at 340 nm. A priori vertical profiles are provided by the TM5-MP daily forecast
305 with a spatial resolution of 1 x 1 degree (Williams et al., 2017). Cloud properties are taken from the S5P operational
306 product Cloud as Reflecting Boundary (CRB; Loyola et al., 2018). In order to correct for any remaining offset and
307 striping due to instrumental artefacts or unknown misfits in the spectral retrieval, a background correction is applied
308 based on HCHO slant columns selected in the emission-free Pacific Ocean. The background HCHO vertical column,
309 due to the methane oxidation, is added using data from the TM5 model in the reference region. We use the quality
310 assurance values (qa_value greater than 0.5) to filter out observations presenting a solar zenith angle larger than 70°
311 or cloud fractions larger than 0.4.

312 The HCHO retrieval fulfils the requirements of the TROPOMI mission (Veeffkind et al., 2012) on accuracy (40-
313 80%) and precision (12×10^{15} molec cm⁻²). The precision of a single observation is estimated to be 5×10^{15} molec cm⁻²
314 in remote locations. The dispersion is naturally larger over polluted sites (from 7 - 10×10^{15} molec cm⁻²). Validation
315 using a global network of FTIR measurements indicates that TROPOMI HCHO columns present a negative bias over
316 high emission sites (-30% for HCHO columns larger than 7.5×10^{15} molec cm⁻²) and a positive bias for clean sites
317 (+20% for HCHO columns lower than 2.5×10^{15} molec cm⁻²) (Lambert et al., 2020; Vigouroux et al., 2020).

318 To characterize the HCHO interannual and seasonal variability, we have used the QA4ECV OMI dataset to construct
319 a climatology based on recent years (2010-2018). This is justified the good agreement between OMI and TROPOMI
320 HCHO columns which is better than 10% for most regions (Lambert et al., 2020). For our analysis, we use two-week
321 averaged columns. This reduces the random uncertainty to about 10%.

322 One of the main drivers of the observed HCHO variability is temperature, which has a direct impact on NMVOC
323 emissions and on the chemical production of HCHO (Stavrakou et al., 2018). It results in a strong correlation between
324 HCHO columns and surface temperatures. For this paper, we correct the HCHO concentrations for this meteorological
325 impact prior to using the data in the analyses. We introduce a temperature correction method (Zhu et al., 2017) based
326 on data from OMI for 2005-2020, and from TROPOMI for 2018-2020. In brief, this correction entails fitting a second-
327 order polynomial through daily HCHO columns reported as a function of the temperature. This novel analysis is
328 performed for each region and on the OMI and TROPOMI time series separately. On this basis, the temperature-
329 induced variations in HCHO are removed from the time series using local daily temperatures specified by ERA5-Land
330 2m meteorological datasets (Muñoz Sabater, 2019a; See Fig. C3). This correction is designed to minimize the impact
331 of temperature fluctuations on the HCHO anomalies. Finally, a polynomial obtained using a climatology of surface
332 temperatures is added to the differential HCHO columns, in order to reintroduce the natural seasonal cycle, assuming
333 the same temperature every year. These temperature-corrected HCHO columns are used throughout this paper. Note
334 that the difference with uncorrected HCHO columns is generally small (less than 10%), but can be significant when
335 looking for small effects such as those induced by COVID-19 related emission changes. The dataset used for this
336 analysis covers the period from May 2018 to June 2020.



337 2.6 Glyoxal (CHOCHO)

338 Glyoxal (CHOCHO) is not one of the TROPOMI operations data products. For this study we used the prototype data
339 product developed as part of the ESA S5p+I GLYRETRO project, which relies on scientific developments performed
340 using the GOME-2 and OMI instruments (Lerot et al., 2010). The algorithm is described in detail in the GLYRETRO
341 ATBD (Lerot et al., 2020). In brief, the retrieval approach consists of a DOAS-type spectral fit for the observed optical
342 depth with reference absorption cross-sections for glyoxal and other absorbing species (NO₂, O₃, O₂-O₂, liquid water
343 and water vapor, and the Ring effect) in the spectral interval of 435–460 nm to derive glyoxal slant column densities.
344 The latter are converted into tropospheric columns using calculated air mass factors, after application of a background
345 correction procedure aimed at reducing possible remaining (row-dependent) systematic biases. Air mass factors are
346 calculated following the formulation of Palmer et al. (2001), which combines box-air mass factors precomputed with
347 the radiative transfer model VLIDORT v2.7 (Spurr and Christi, 2019) and a priori glyoxal concentration profiles
348 provided by the MAGRITTE chemistry-transport model (Müller et al., 2018, 2019).

349 The glyoxal optical depth is very small ($< 5 \times 10^{-4}$), which makes its retrieval very sensitive to instrumental noise and
350 to interferences with spectral signatures of species absorbing more significantly in the same spectral region. The first
351 factor introduces large random errors, in the range $6\text{--}10 \times 10^{14}$ molec cm⁻², which can however be reduced by spatial-
352 temporal averaging, that is, using multiple observations averaged time and/or space. Systematic uncertainties are
353 dominated by spectral interferences, but also by uncertainties associated with the auxiliary data used as an input for
354 the AMF calculation. These uncertainties are estimated to be $2\text{--}3 \times 10^{14}$ molec cm⁻² (~50% for source regions). To limit
355 uncertainties related to cloud contamination, glyoxal observations are only provided for scenes with effective cloud
356 fractions smaller than 20% (taken from the operational NO₂ product). As with HCHO, to account for seasonal and
357 interannual variability, a climatology of OMI CHOCHO columns was built to further delineate sources of variability
358 for glyoxal column amounts.

359 Validation of satellite glyoxal column observations is generally limited, mostly due to the scarcity of independent
360 ground-based data. However, a preliminary validation based on a few MAX-DOAS stations in Asia and Europe,
361 indicates that the satellite and ground instruments measure consistent glyoxal tropospheric column amounts with mean
362 differences generally less than 2×10^{14} molec cm⁻², except in particular conditions such as low sun elevation or for
363 stations that are frequently covered by clouds (Alvarado et al., 2020). The dataset used for this analysis covers the
364 period from May 2018 to June 2020.

365 3 Global Observations of Nitrogen Dioxide

366 TROPOMI measurements of tropospheric NO₂ column amount are well-suited for detecting emission from a variety
367 of anthropogenic sources including traffic, power plants, and industry. The atmospheric lifetime of NO₂ and its vertical
368 profile shape dictate that the high spatial resolution measurements from TROPOMI can readily capture rapid week-
369 to-week changes in near-surface emissions from COVID-19 impacted cities and point sources. To give context and
370 overview, the global distribution of tropospheric NO₂ based on an annual average for 2019 with an oversampling
371 resolution of approximately $0.02^\circ \times 0.02^\circ$ is illustrated in Figure 1. The high resolution of these measurements enables

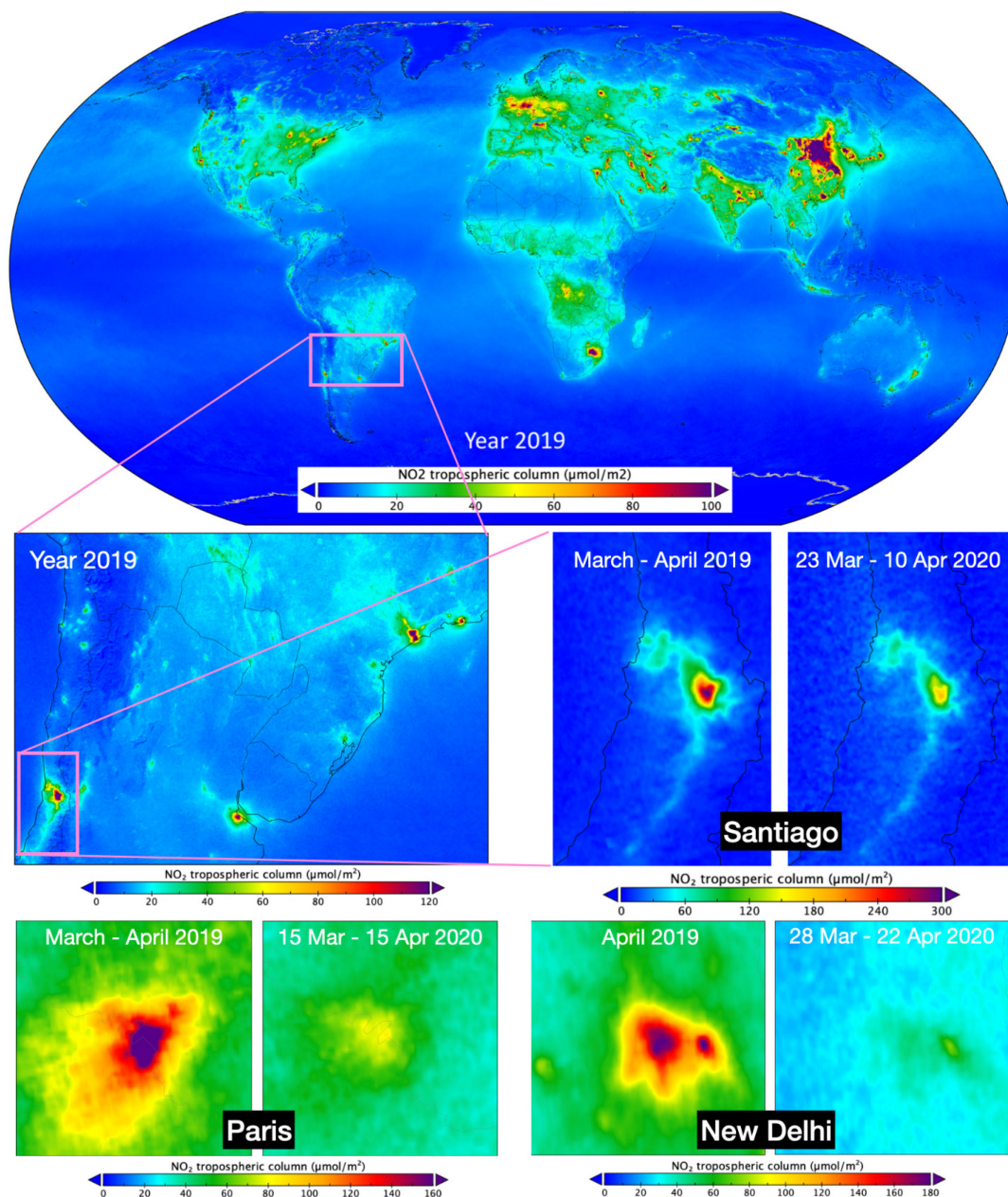


372 further zooming to the regional, suburban, and city scale providing detailed information about spatial distributions. A
373 regional zoom-in over central South America reveals high NO₂ levels over the megacities of Rio de Janeiro, São Paulo,
374 Buenos Aires, and Santiago. A further zoom-in to central Chile and its capital Santiago is shown in Figure 1, focusing
375 on a shorter period from 23 March to 10 April 2020, which coincides with a region-specific COVID-19 lockdown
376 (Figure 2k), as compared to the mean tropospheric NO₂ column for March-April 2019. Note that the period in 2019
377 is chosen to be longer than 2020 in order to reduce the effects of natural variability, but the period is centered at the
378 beginning of April to avoid the influence of the seasonal NO₂ cycle. A strong reduction in the NO₂ tropospheric
379 concentration of about 40% is observed over Santiago during this period, and a 28% reduction is observed between
380 23 March and 15 May corresponding to the period when restrictions were eased (Figure 2k). Interestingly, a further
381 zoom shows that the relative reduction is not uniform over the city, reflecting differences in the mix of source
382 contributions for the different quarters of the city.

383

384

385



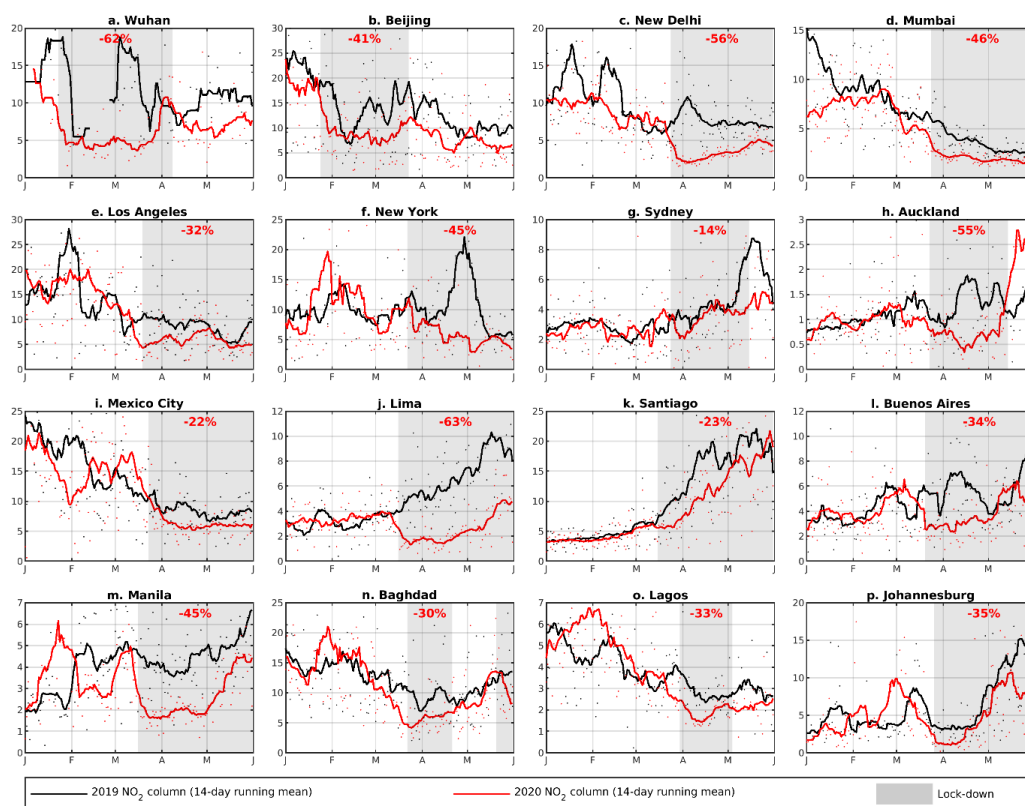
386

387 **Figure 1:** Global distribution of NO₂ based on the annual average of tropospheric column amounts of NO₂ measured by
388 TROPOMI for 2019 (top panel) shown in units of micromole per m². Using the same data, several zoom-in plots are shown
389 in the middle and bottom panels: regional zoom-in for central South America (middle left) and a city-scale zoom-in over
390 Santiago, Chile (middle right panels, comparing 23 March to 10 April 2020 with March-April 2019), over Paris (lower left,
391 comparing 15 March to 15 April 2020 with March-April 2019) and over New Delhi (lower right, comparing 28 March to 22
392 April 2020 with April 2019). Note the different color scales in the three subpanels. The domain size of the panels is 1.5 x 1.0
393 degree for Paris, and 1.1 x 1.0 degree for New Delhi.



394
395
396
397
398
399
400
401
402
403
404

Two more examples of lockdown-related NO₂ column reductions in major cities are shown for Paris and New Delhi in Figure 1 with time windows selected to reflect region-specific lockdown periods. In Paris, the NO₂ levels for the period 15 March to 15 April 2020 are about a factor of two lower than in March-April 2019 (see also Figure 4). For New Delhi the reduction is even more striking in comparison to April 2019 (about a factor of 3, Figure 2c). Both Paris and New Delhi also show significant reductions in background values around the cities. Background locations are subject to a variety of wind directions and sometimes downwind of city plumes thus influencing background concentrations. Such plumes are typically on the order of 100 km long, and, given the atmospheric residence time of NO₂ (2-12 hours), these plumes can fill the small domains around Paris and New Delhi shown in Figure 1.



405
406
407
408
409
410
411

Figure 2: Time series of TROPOMI NO₂ column amounts (in 10¹⁵ molec cm⁻²) for selected cities for the period 1 January to 1 June in 2019 (black dots) and 2020 (red dots). TROPOMI observations are averaged over a 25 x 25km² box around the city center. The lines indicate the two-week running mean for 2019 (black) and 2020 (red). The grey zones indicate the official lockdown period for each city. The reduction of the average NO₂ column during the lockdown period relative to the same period in 2019 is given inset. Details about the lockdown dates are summarized in Table C2.



412 The lockdown periods and the measures taken to mitigate the spread of the COVID-19 were rolled out on a country-
413 and often city-specific basis. Figure 2 illustrates the temporal evolution of NO₂ tropospheric columns from January to
414 May over large cities for different continents. The observed reductions in China and India are discussed in more detail
415 in Sect. 4 and 5. Detailed information about the lockdown measures adopted for those cities is given in Table C2. The
416 TROPOMI observations indicate substantial decreases in NO₂ during the lockdowns in all studied cities, but the
417 reductions vary significantly from one city to another.

418 In Wuhan, the first city to issue quarantines and lockdown measures, the observed NO₂ column drastically declined
419 (-60%) between 23 January and 8 April 2020 compared to the same period in 2019 (Table C2). This decrease is in
420 good agreement with estimated reductions for the period 11 February to 2 March 2020 based on TROPOMI NO₂ (-
421 43%, Bauwens et al., 2020) and in situ NO₂ observations in Wuhan (-55%, Shi and Brasseur, 2020). However, it
422 should be noted that there was strong day-to-day variability in the NO₂ column amount due to meteorological factors,
423 as well as missing data over Wuhan in February 2019 due to clouds. Model calculations by Liu et al. (2020) indicate
424 that meteorological variability could have led to increased NO₂ columns in 2020 compared to 2019, suggesting that
425 the observed NO₂ reductions underestimate the impact of emission reductions due to COVID-19. The partial lifting
426 of the restrictions on 8 April led to a progressive increase in NO₂ levels, yet remained lower than in 2019, likely
427 because the population was still advised to stay at home and schools remained closed. A similar response in NO₂
428 levels was observed in Beijing. The decreases were less pronounced (-40%) and are in excellent agreement with the
429 reported decrease based on in situ NO₂ measurements (-40%, Shi and Brasseur, 2020). The weaker response could be
430 due to the less drastic measures adopted in Beijing, because locally sustained COVID-19 cases were lower than in the
431 Hubei province (Leung et al., 2020). Strong NO₂ reductions were observed for other Chinese cities, like Nanjing,
432 Qingdao, and Zhengzhou, based on TROPOMI NO₂ observations (Bauwens et al., 2020).

433 India enforced strict restrictions of human activities on 24 March 2020 to tackle the spread of COVID-19. In New
434 Delhi and Mumbai, the onset of the lockdown induced a sharp decline in the observed NO₂ columns (by a factor of
435 2). The columns remained low during the entire lockdown period (-56% and -46%, respectively) (see Table 2 for
436 timing of lockdown phases). This is very much in line with the decreases reported in New Delhi based on NO₂ data
437 from monitoring stations, -53% (Mahato et al., 2020) and -48% (Jain and Sharma, 2020).

438 As compared to other cities, a very strong NO₂ decrease was observed in Lima (-63%), where strict regulations to
439 stay indoors were enforced (Collins, 2020). A drastic drop in NO₂ compared to the 2019 levels marked the start of
440 the lockdown, and the levels remained very low throughout the entire lockdown period. The gradual increase of NO₂
441 columns in Lima and other Southern Hemispheric cities from January to May (Figure 2) reflects the natural seasonal
442 variation when levels peak during the Southern Hemispheric winter, as temperatures decrease and NO₂ lifetime
443 increases.

444 In Buenos Aires, the observed reduction was not as strong compared to Lima for the entire lockdown period (-34%,
445 Table C2), but was particularly marked during the first month of the lockdown (20 March through 20 April 2020),
446 due to a compulsory quarantine period and strict limitation of activities for many sectors. Although partial lifting of
447 measures was issued after 10 April for many provinces in Argentina, the measures in the Buenos Aires agglomeration
448 were maintained due to the elevated number of cases (Raszewski and Garrison, 2020). More moderate reductions are



449 found for Mexico City (-22%) and Santiago (-23%) during the lockdown in comparison to the same period in 2019,
450 that could be attributed to less strict adherence to and enforcement of lockdown measures (Uchoa, 2020; Pasley, 2020).

451 Strong reductions were observed over the entire lockdown period in the heavily hit cities in southwest Europe, Los
452 Angeles, and New York, with reductions ranging between -32% and -54% (Bauwens et al., 2020). It should be noted
453 however, that in these regions, the start of the lockdown period is generally less marked partly because the lockdowns
454 were not as strictly enforced in Europe and the U.S. as in China and India. Moreover, the observed TROPOMI data
455 displays a strong variability attributable to meteorology, e.g. over Paris, New York and Los Angeles in 2019.

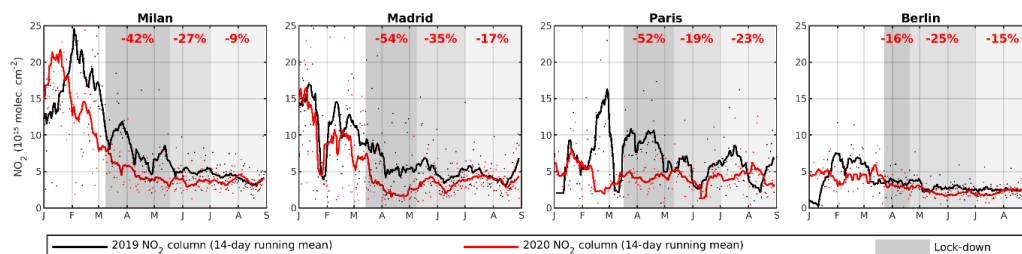
456 In Sydney, the reduction was moderate (-14%) and delayed with respect to the onset of the measures (Figure 2).
457 This could be related to observations of less strict compliance in the early period of lockdown measures (New South
458 Wales Public Health, 2020). A rapid and strong decrease was observed for NO₂ column amount as a result of lockdown
459 measures in Auckland, New Zealand (-55%). Similarly, the lockdown measures in New Zealand were implemented
460 swiftly with high levels of compliance (Matthews, 2020). The end of the lockdown coincided with a strong increase
461 in NO₂ pollution, from 1.8×10^{15} molec cm⁻² to 3×10^{15} molec cm⁻² in the last three weeks of May.

462 In Africa, Nigeria is among the countries most affected by COVID-19 and reported the first confirmed case in sub-
463 Saharan Africa (Odunsi, 2020; Adigun and Anna, 2020). A two-week lockdown period was put in place for Lagos
464 starting 30 March. The NO₂ column amount decreased by 33% during the lockdown (Figure 2) with respect to the
465 same period of 2019 and remained lower even after the lifting of restrictions on 4 May (Table C2). An NO₂ column
466 decrease of similar magnitude (-35%) was observed in Johannesburg, where a national lockdown was issued on 26
467 March 2020, with a gradual easing of restrictions starting 1 May. In Sub-Saharan Africa, the emission reductions in
468 April were significant for larger populous and industrialized areas, whereas no noticeable drop was found in less
469 developed regions (Masaki et al., 2020).

470 Finally, the Iraqi capital of Baghdad faced an initial lockdown from 22 March through 21 April. A second partial
471 lockdown was issued starting 20 May in response to a sharp increase in COVID-19 cases due to the temporary
472 relaxation of restrictions to allow the celebration of Ramadan in late April (Table C2). The NO₂ column responded
473 quickly (Figure 2n) as confirmed by the rapid decrease once curfew measures were issued in late-May.

474 Figure 3 and Figure 4 illustrate the tropospheric concentration of NO₂ over Europe, focusing on Milan, Madrid,
475 Paris and Berlin (Figure 3), extending the analysis to include summer months. In France, Spain and Italy we detect
476 strong reductions of NO₂, which can be largely attributed to the lockdown measures. In Berlin, the measured
477 differences are smaller, and a more detailed analysis of the meteorological variability is needed to quantify the impact
478 of the lockdown (see Figure 3). The extended time series shows a recovery of the NO₂ pollution levels to pre-COVID-
479 19 values. However, the recovery is not complete, suggesting that remaining restrictions, new stay-at-home life and
480 working practices, together with a downturn in industrial and service-based activities have contributed to a longer
481 lasting impact.

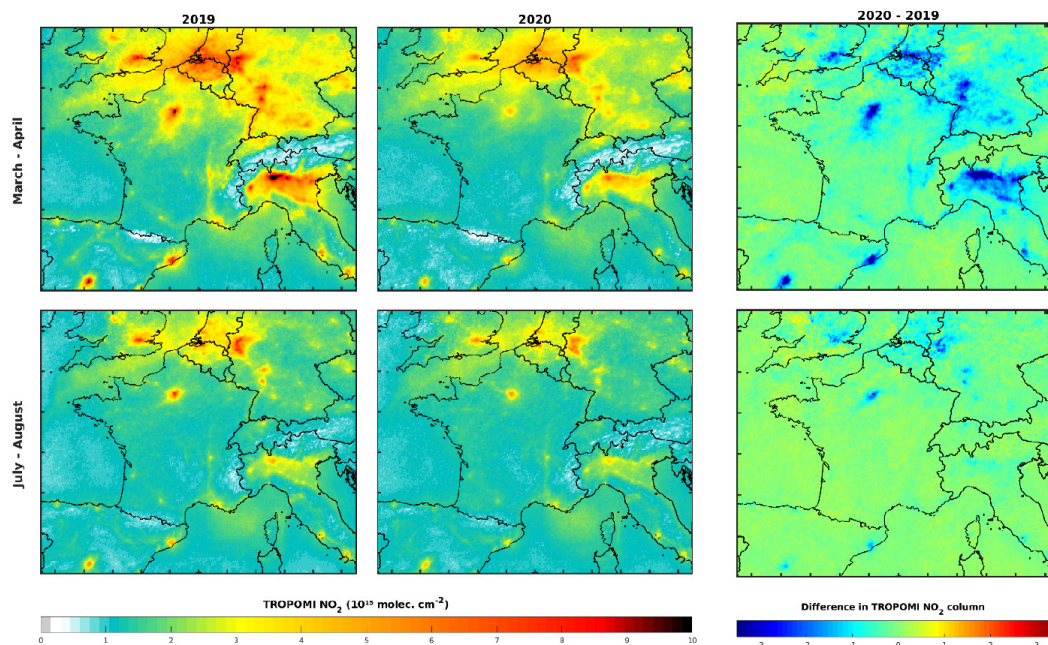
482
483



484

485 **Figure 3:** Same as Figure 2, for the European cities Milan, Madrid, Paris, and Berlin, for an extended period of 1 January
486 to 1 September. Additional shading indicates the lockdown period (dark grey), a transition period (grey), and the period
487 with relaxed regulations (light grey).

488



489

490 **Figure 4:** TROPOMI NO₂ tropospheric columns over Europe in the lockdown months March-April (top) and the post-
491 lockdown months July-August (bottom), comparing 2019 (left) with 2020 (middle). The difference is shown in the right
492 panel.

493

494 Relative concentration changes between 2019 and 2020, as mentioned previously, should not be fully attributed to
495 COVID-19 lockdown measures and the subsequent reduction of emissions. Daily changes in the weather have a strong
496 influence on the NO₂ concentrations, even when the data is averaged over a month. In order to estimate the impact of
497 meteorological variability on TROPOMI-based NO₂ observations, simulations were performed with the LOTOS-
498 EUROS chemistry-transport model over Europe at a resolution of 0.1° x 0.1°. Using the same emissions for 2019 and
499 2020, the simulations show that meteorological variability is responsible for changes in the monthly-mean, city-



500 averaged NO₂ columns with a 1-sigma standard deviation of about 13%. This variability is clearly illustrated in e.g.
501 the individual daily observations in Figure 2. The drastic changes in the range of 30-60% observed in the TROPOMI
502 data and shown in Figure 1 through Figure 4 clearly fall outside this range and cannot be attributed to weather alone.

503 A second complication is the presence of clouds. Months with persistent local cloud cover will therefore have a
504 reduced number of tropospheric column observations and will exhibit more natural variability. For quantitative
505 estimates of the COVID-19 measures, these factors should be carefully taken into account. This can be done through
506 (i) daily-based analysis of the NO₂ plumes from cities using wind speed fields from meteorological models and
507 subsequent emission derivation (Lorente et al., 2019; Goldberg et al., 2019); (ii) regression models to estimate the
508 impact of natural variability and emission trends in the observations (Diamond and Wood, 2020); (iii) chemistry-
509 transport modelling (Chang et al., 2020; Liu et al., 2020; Barré et al., 2021); and (iv) inverse modelling and data
510 assimilation approaches (Ding et al., 2020; Miyazaki et al., 2020).

511 **4 Regional Observations for China**

512 China was the first country to impose measures to limit the spread of the SARS-CoV-2 virus. Although no national
513 lockdown was declared, strict local lockdown measures were implemented in many cities and provinces. In Wuhan,
514 the epicenter of the virus outbreak, the lockdown period lasted from 23 January 2020 until 8 April 2020, while in other
515 regions, it generally started in early February with measures being eased and lifted through March. In addition to the
516 lockdown measures, the yearly Chinese New Year holidays also affected the amount of anthropogenic emissions (Tan
517 et al., 2009), and so needs to be considered for proper interpretation of the observations. The timing of the holiday
518 period differs from year to year and took place from 24 January to 2 February in 2020, and in the periods 4-10 February
519 and 15-21 February for 2019 and 2018, respectively.

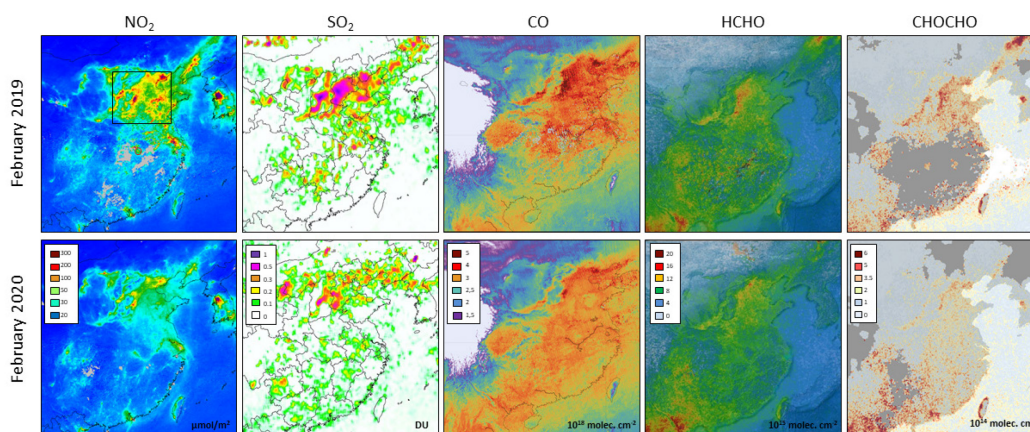
520 The impact of the COVID-19 crisis on air quality in China has already been investigated in several studies. Bauwens
521 et al. (2020) reported that tropospheric NO₂ column amounts observed by TROPOMI during the lockdown dropped
522 by 40-50% in the most impacted cities compared to the same period in 2019 (see Sect. 3). Accordingly, top-down
523 estimated NO_x emissions exhibited sharp reductions of up to 50% during the strict lockdown period in late January
524 through early February (Ding et al., 2020; Liu et al., 2020; Zhang, R. et al., 2020).

525 In situ data indicate significant reductions of ground concentrations for NO₂, but also for PM, SO₂, and CO (Shi and
526 Brasseur, 2020; Wang et al., 2020; Zhang, Z. et al., 2020; Zhao, Y. et al., 2020). On the other hand, those studies
527 consistently reported increases of ozone concentrations. With the support of models, Zhao, Y. et al. (2020) have shown
528 that the observed decreases in NO₂ concentration were mostly caused by emissions reductions. They also show that
529 the contribution of meteorological changes to the observed concentration reductions of other species depends on the
530 exact location. Based on OMI observations, Zhang, Z. et al. (2020) observed reductions in East Asia of about 33%
531 and 41% for NO₂ and SO₂, respectively.

532 City-scale impacts of lockdown on NO₂ tropospheric column amounts for Wuhan and Beijing in Sect. 3. Here, we
533 investigate whether a lockdown signature can be detected from space at the regional scale for other key pollutants by
534 focusing on TROPOMI tropospheric column measurement of SO₂, CO, HCHO, and CHOCHO. We also compare the
535 identified changes with the marked changes in NO₂ concentration. Figure 5 compares monthly mean tropospheric



536 columns of those different species for February 2019 and 2020. The NO₂ and SO₂ tropospheric column amounts are
537 clearly lower in February 2020 compared to 2019. A small general reduction is also visible in the CO, HCHO and
538 glyoxal column amounts. As discussed before, many factors other than the lockdown measures may explain changes
539 in pollutant concentrations, such as the meteorology or emission reduction related to the timing of holidays. Another
540 difficulty to compare different years is the data sampling. In February 2019, large parts of Southern China were
541 covered by clouds, preventing space-based observation of the lowermost atmospheric layers. This is clearly illustrated
542 in the upper panel of Figure 5 showing CHOCHO concentrations, where data is missing over large regions since this
543 product uses the most stringent cloud filtering as compared to the other trace gases. Therefore, the following detailed
544 discussion only focuses on the northern part of China (black box in Figure 5 top left panel), even though the lockdown
545 measures were stricter in the region of Wuhan.
546
547

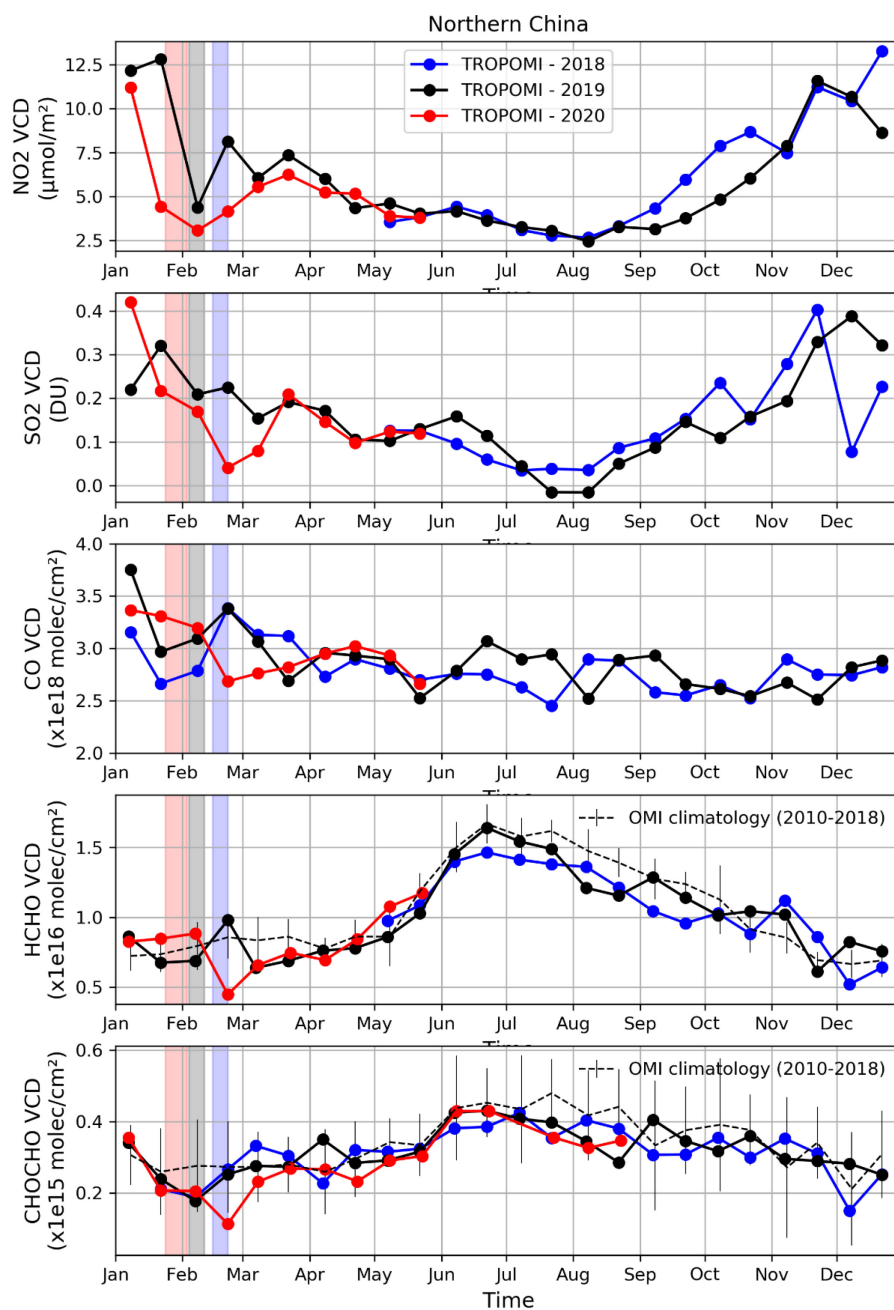


548
549 **Figure 5: Tropospheric and total columns for various trace gases over China as observed by TROPOMI over China in**
550 **February 2019 (upper panels) and 2020 (lower panels). The black box indicates the geographical region used in the time**
551 **series analysis (Figure 6). Note: the grey-shaded regions in NO₂ and CHOCHO panels (far left and far right, respectively)**
552 **indicate areas with little or no data available due to persistent local cloud cover.**

553
554 Figure 6 shows the seasonal cycles for tropospheric column amounts of TROPOMI NO₂, SO₂, CO, HCHO, and
555 CHOCHO for different years in northern China (region in black box highlighted in Figure 5) starting at the beginning
556 of the operational phase of the S5P/TROPOMI mission (30 April 2018). The different colored curves show two-week
557 medians of the daily mean tropospheric columns. In order to focus on the effect of COVID-19 lockdown measures for
558 HCHO and CHOCHO, the TROPOMI-based time series are compared with an OMI-based climatology for these
559 species using OMI data from 2010 to 2018, and shown by the black dashed curves. The associated uncertainties
560 represent the interannual variability as estimated from OMI. This type of climatological reference based on a longer
561 time series is not available for CO. Therefore, Figure 6 shows CO columns starting from 1 January 2018, which have
562 been added to extend the time series even though the data sampling was more limited in the early phase of the mission.



563 The light vertical boxes in January and February indicate the period of Chinese New Year holidays. Note that the 2020
564 holiday period was slightly extended as a first measure against the COVID-19 spread.
565
566



567



568 **Figure 6: Two-week median tropospheric column concentrations of NO₂, SO₂, CO, HCHO and CHOCHO (from top to**
569 **bottom) for northern China (34°N-40°N; 110°E-120°E). The different curves represent different years as indicated in the**
570 **legend. The colored boxes represent the yearly Chinese New Year holidays for those same years. The dashed black lines in**
571 **the HCHO and CHOCHO panels represent a climatological seasonality as obtained using the OMI data sets from 2010 to**
572 **2018 and the error bars represent the interannual variability (1-sigma standard deviation).**

573

574 Superimposed on the overall seasonal cycle of NO₂ (maximum during wintertime caused by a longer atmospheric
575 lifetime), a clear reduction of the NO₂ columns is systematically observed which corresponds to the New Year
576 festivities. While a quick return to higher values is usually observed after that period (Tan et al., 2009), the NO₂
577 columns remained lower for several weeks in 2020 likely as a consequence of the reduced traffic and industrial
578 activities. For example, NO₂ column amounts at the end of February were about 45% lower than those of 2019. In
579 March 2020, NO₂ columns return progressively to a similar level as compared to other years.

580 SO₂ emissions in China mostly originate from fossil fuel burning of coal and oil (Wang et al., 2018). Although
581 Chinese SO₂ emissions have dropped significantly in the last decade (van der A et al., 2017; Zheng et al., 2018a),
582 enhanced SO₂ columns are still observed in some regions of northern China (Figure 5). As illustrated in Figure 6, SO₂
583 column amounts are larger during wintertime mostly due to its longer atmospheric lifetime (Lee et al., 2011). No clear
584 reduction could be related to the yearly holidays. However, in 2020 a sharp drop is observed starting in late January
585 through mid-March with a reduction of up to 77% as compared to 2019. By late-March/early-April values returned to
586 levels similar to previous years, which is consistent with the NO₂ lockdown signature.

587 In northern China the residential sector, consisting of mostly of emissions from heating and cooking, accounts for
588 nearly half of the anthropogenic CO emissions, while the rest is distributed between traffic, power generation, and
589 industry (Zheng et al., 2018b). Since the impact of lockdown measures is more limited for the residential sector as
590 compared to the transport or industrial sectors, the response of CO to the lockdown measures is expected to be less
591 distinct. Also, due to the longer atmospheric lifetime of CO (weeks to a month), the observed column amounts result
592 from the accumulation of the trace gas over source regions and from long-range transport from regional and global
593 sources. As such, meteorology significantly influences CO concentrations. The observed day-to-day variability is
594 indeed large, leading to more scatter in the two-week median time series shown in Figure 6. The CO columns observed
595 in late February/early March are lower than those observed in the last two years, which might be partly caused by the
596 lockdown measures. However, the high temporal and spatial natural variability of the CO column amount is of the
597 same magnitude as the possible COVID-19 lockdown signal, and the large, year-to-year interannual differences
598 prevent firm conclusions from being drawn. Dedicated model simulations or a longer time series of the TROPOMI
599 CO data may help to disentangle these effects in the future.

600 There are difficulties associated with the investigation of a possible lockdown signature in the satellite HCHO and
601 CHOCHO data sets. Large uncertainties are associated with both of these column retrievals owing to their low optical
602 depth. Moreover, HCHO and CHOCHO columns are dominated by biogenic emissions, which explains the observed
603 seasonal pattern of HCHO and CHOCHO column values with a maximum during summertime as illustrated in Figure
604 6. Variability in meteorology (temperature changes, winds, precipitation) may lead to changes in column amounts on
605 the same order of magnitude as the expected lockdown-related reduction in anthropogenic emission changes. The
606 interannual variability as inferred from the OMI data sets is estimated to be in the range of 1×10^{14} molec cm⁻² (~30%)



607 and 1.2×10^{15} molec cm^{-2} (~12%) for CHOCHO and HCHO, respectively. Despite those issues, a clear minimum is
608 visible for both HCHO and CHOCHO in late February 2020, with columns significantly lower than 2019 and lower
609 than the OMI climatology (about -40% and -50% for HCHO and CHOCHO, respectively). The differences are also
610 larger than what can be explained by the typical interannual variability. This is in agreement with Sun et al. (2021),
611 who finds a significant HCHO decrease in the Northern China Plain. For glyoxal, a reduction of the column amounts
612 starts already in late January but similar reductions are observed in other years and might be related to a holiday effect
613 similar to that observed for NO_2 .

614 It is interesting to note that local minima are observed simultaneously in late February 2020 for all species except
615 NO_2 , despite the data products being generated using independent retrieval algorithms. This gives confidence into the
616 detected reductions and their anthropogenic origin. The small delay between the initial decrease in NO_2 concentration
617 and the observed decreases in the other trace gas signals is related to a combination of longer atmospheric lifetimes
618 and production being dominated by secondary processes as compared to NO_2 and is also likely tied to the early timing
619 of the Chinese New Year in 2020.

620 5 Regional Observations for India

621 India implemented strict national lockdown measures limiting activities across the country starting 24 March 2020 for
622 a period of 21 days in order to tackle the spread of the SARS-CoV-2 virus amongst its 1.3 billion inhabitants. The
623 initial stringent phase 1 restrictions were followed by careful region-based relaxations in three subsequent phases
624 carried out through the end of May as shown in Table 2.

625

626 **Table 2: Lockdown phases in India.**

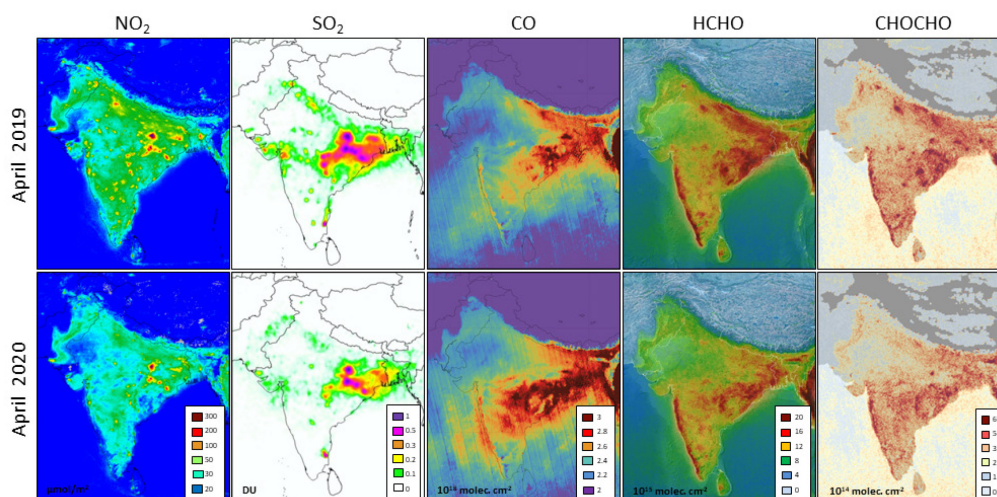
	Dates	Measures	Reference
Phase 1	24 Mar to 14 Apr	Nearly all services and factories suspended.	Singh et al. (2020)
Phase 2	15 Apr to 3 May	Extension of lockdown with relaxations, reopening of agricultural businesses and small shops at half capacity.	BBC News (2020)
Phase 3	4 May to 17 May	Country split in 3 zones: (i) lockdown zone, (ii) zone with movement with private and hired vehicles, and (iii) normal movement zone.	India today (2020)
Phase 4	17 May to 31 May	Additional relaxations, more authority given to local bodies.	The Economic Times, 2020

627

628



629 Figure 7 gives an overview of TROPOMI observations of NO₂, SO₂, CO, HCHO, and CHOCHO, over India for
630 April 2020, thus covering most of phase 1 and 2 of the Indian lockdown, as compared to the same month in 2019. For
631 NO₂ and SO₂ the concentrations are clearly lower across the country in 2020 as compared to 2019. Although less
632 prominent, concentrations of CO, HCHO, and CHOCHO appear to be lower in April 2020 over the domain of the
633 Indo-Gangetic Plain (IGP), which is one of the most densely populated areas of the world with roughly 900 million
634 people.
635
636



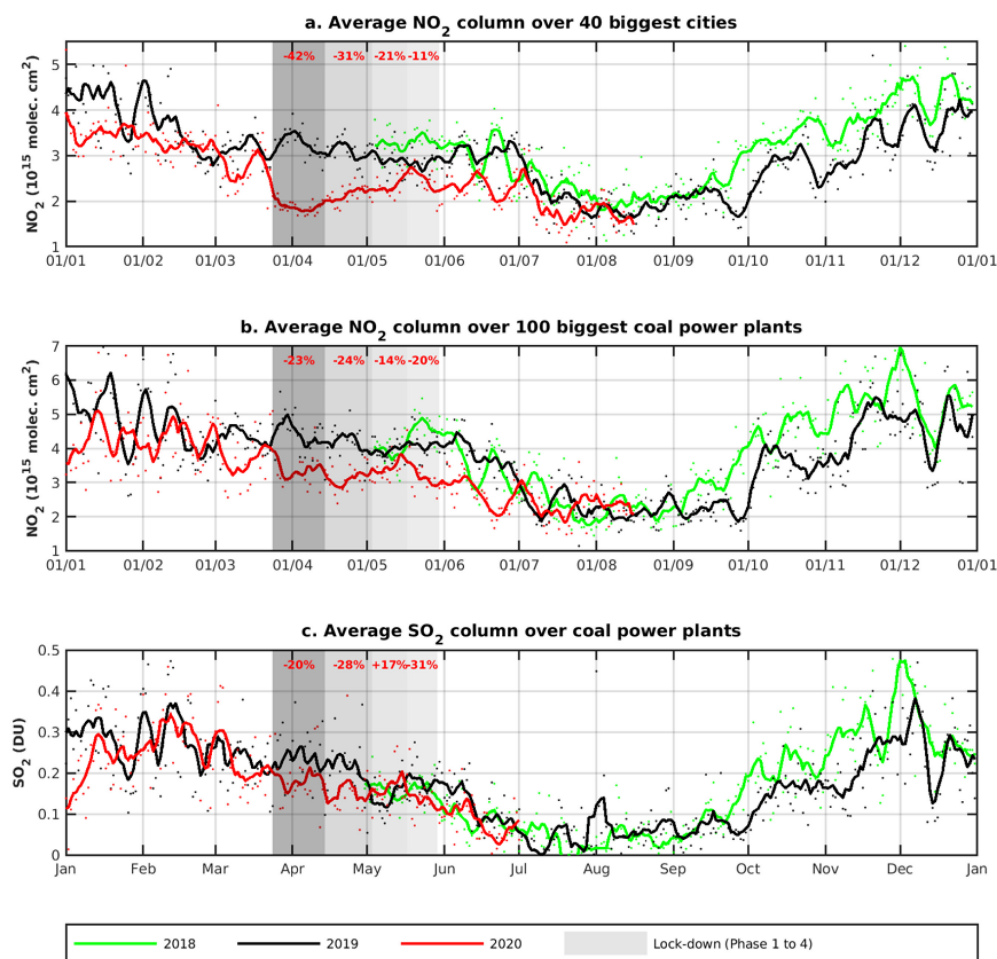
637
638 **Figure 7: Concentrations maps for April 2019 (top row) and April 2020 (bottom row) for the various trace gas species**
639 **measured by TROPOMI from left to right, NO₂, SO₂, CO, HCHO and CHOCHO.**

640
641 The two main sources of NO₂ are road transport and power generation, each accounting for about 30% of total
642 anthropogenic emissions in India (Granier et al., 2019). During phase 1 of the lockdown the Tom-Tom traffic index
643 dropped by 80% (Aloi et al., 2020; Prabhjote, 2020) and energy consumption dropped by 25% compared to 2019
644 (Dattakiran, 2020; POSOCO, 2021) (Fig. D1). As such, we expect a strong reduction in NO₂ particularly in urban
645 areas due to large decreases in transport sector activities and we expect a weaker reduction near power plants due to
646 smaller decreases in energy demand.

647 Indeed, as indicated by the maps of NO₂ column concentrations in Figure 7, a notable reduction in NO₂ can be seen
648 in April 2020 as compared to April 2019. A clear reduction is observed over major cities as well as over the eastern
649 part of India where most large power plants are located. Figure 8a shows the average NO₂ total column concentrations
650 as measured by TROPOMI for 2018, 2019 and 2020, for the 40 largest cities in India selected on the basis of the
651 number of inhabitants (www.geonames.org) where NO₂ is averaged over a 15 x 15 km² area around each city center.
652 When both city centers and power plants are located within a 45 x 45 km² box, this box is excluded from the averages
653 to avoid potential outflow of one source to the other. A sharp reduction of 42% can be seen in the amount of NO₂ over



654 cities during the first phase of the lockdown period starting at the end of March, as compared to the same period in
655 2019. This initial drop in NO_2 is then followed by a slow but gradual increase in line with the successive relaxation
656 phases (Table 2). Power generation is a major source for NO_2 in India, in particular from coal-fired power plants.
657 When examining the average amount of NO_2 over the 100 largest coal-fired power plants (www.wri.org), we observe
658 a significant drop in NO_2 during phase 1 of the lockdown period. This drop, observed over coal-fired power plants of
659 23% as compared to 2019 (Figure 8b), is less pronounced than the observed drop in NO_2 over cities (Figure 8a). The
660 TROPOMI-observed reduction in NO_2 over coal-power plants is in line with the initial 25% decrease in maximum
661 electricity demand reported by National Load Dispatch Centre (NLDC) during phase 1 and tapering to an 8% decrease
662 during phase 4 of the lockdown as compared to 2019 (Fig. D1, Dattakiran, 2020).
663



664
665 **Figure 8:** Average tropospheric NO_2 concentrations for May 2018 (green), 2019 (black) until June 2020 (red) over the 40
666 largest Indian cities (top); over the 100 largest power plants in India (middle); and average SO_2 concentrations over the
667 59 largest SO_2 -emitting power plants in India (bottom). The four different phases of the lockdown period are denoted by



668 **the different grey shading. For each phase, the reductions in NO₂ (or SO₂) concentrations are given relative to the same**
669 **period in 2019. The dots are the daily means, and the solid lines represent the 7-day running means.**

670

671 According to the CAMS-GLOB-ANT emission inventory for 2019 the major sources for SO₂ in India are power
672 generation (65%) and industry (25%) (Granier et al., 2019). Since India largely relies on coal for producing energy, it
673 is the world's top emitter of anthropogenic SO₂ (Li et al., 2017). So, most of the SO₂ signal we see in TROPOMI data
674 for this region (Figure 7) is from coal-fired power plants, where contributions from oil and gas plants in India comprise
675 a much smaller part of the signal (Fioletov et al., 2016). From Figure 7, a reduction in SO₂ is visible over most areas,
676 and is especially noticeable for the easternmost part of India, which is India's largest SO₂-emitting region with more
677 than 20 coal-fired power plants.

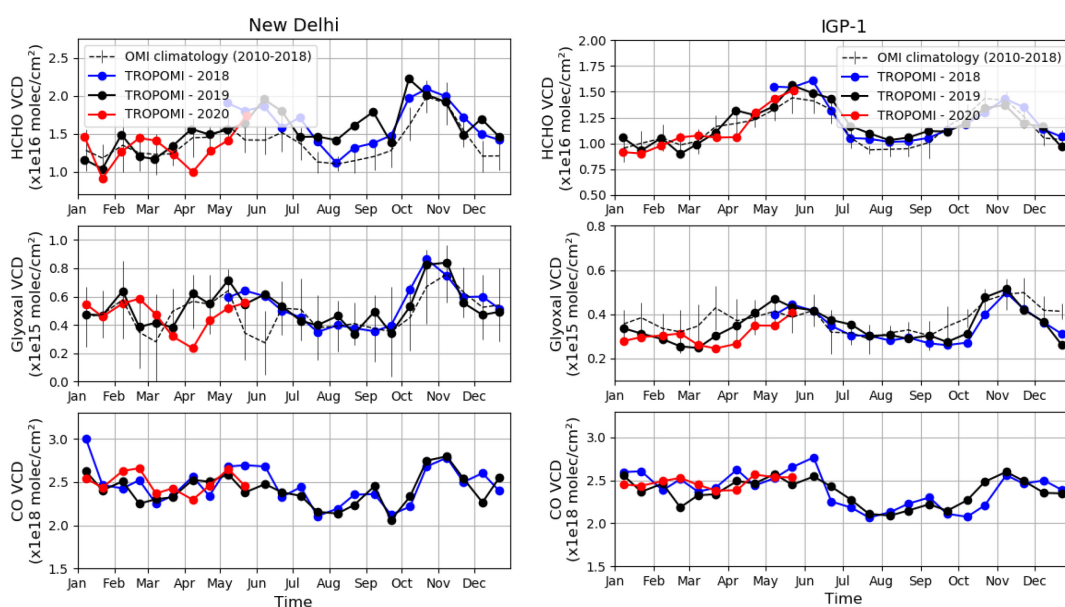
678 We have investigated the SO₂ VCD amounts over the largest power plants, and adapted the selection method used
679 for NO₂ by considering a larger area of 50 x 50 km² around each power plant. This is justified by (1) the longer lifetime
680 of SO₂ compared to NO₂, (2) the lower contamination by other sources, and (3) the need to reduce the noise on the
681 SO₂ data to more clearly isolate the signal from the power plant. The results of the averaged SO₂ VCD time series are
682 presented in Figure 8c. It should be noted that, compared to NO₂, an additional selection of the power plants was
683 applied. Based on the SO₂ VCD map for April 2019 (Figure 7), only the power plants with mean SO₂ columns larger
684 than 0.15 DU were considered (59 power plants in total). Although the signal is relatively weak for SO₂, we find very
685 similar reductions in SO₂ as compared to NO₂. Especially during the first two phases of the lockdown, a reduction of
686 about 20% is found which is in line with the NO₂ observations and the reported reduction in energy demand. In May,
687 for the different years, the consistency between NO₂ and SO₂ VCDs is less straightforward and the reason for this is
688 not fully understood. It should however be noted that the NO₂ and SO₂ data products do not use the same cloud
689 products for filtering and this might be a reason for discrepancy. Moreover, the possibility of a systematic
690 contamination of the NO₂ signal over power plants by other sources cannot be ruled out completely. A noticeable
691 feature of Figure 8b and Figure 8c is the overall excellent correspondence between NO₂ and SO₂ VCD evolution (on
692 short-term/seasonal basis, and outside the lockdown periods) as well as from year to year. This further strengthens the
693 observed COVID-19 related drop in both trace gases, although it is clear that meteorology and chemistry likely play
694 a large role in the observed VCD variability. Also, ground-based studies in New Delhi find a more important reduction
695 in NO₂ compared to SO₂ (Mahato et al., 2020; Kumari and Toshniwal, 2020).

696 For HCHO, CHOCHO, and CO, various regions over India have been investigated to detect a possible signal
697 resulting from COVID-19 lockdown measures. We could only identify such a signal in the densely populated areas of
698 the Indo-Gangetic Plain and New Delhi. These areas, due to the high intensity of traffic and industrial activities, are
699 most likely to exhibit large impacts on atmospheric pollution levels due to COVID-19 lockdown measures.

700 Figure 9 shows two-week averaged column values for HCHO, CHOCHO, and CO over the IGP and New Delhi,
701 based on TROPOMI data from January 2018 to June 2020. To support the interpretation of the observed seasonal and
702 interannual variations, Fig. D2 presents the corresponding temperature, precipitation amount, and fire count. The
703 temperature starts increasing in January and reaches a maximum in June. The period from July to September
704 corresponds to the monsoon season with heavy rains and lower temperatures, and therefore lower pollution levels.
705 Fire activity peaks around May with a second peak is observed in November for the IGP. The time series of the HCHO,



706 CHOCHO, and CO columns correlate with these seasonal events, although with a different amplitude. For example,
707 HCHO shows the strongest correlation with temperature (see Sect. 2.5), while CHOCHO mainly follows fire
708 emissions. The smaller amplitude in CO variations is caused by its longer lifetime.
709
710



711

712 **Figure 9:** Time evolution of HCHO, CHOCHO, and CO over the densely populated Indo-Gangetic plain (defined by the
713 region within this 4 coordinates: 29.5°N 72°E, 21.5°N 86°E, 24.5°N 88.5°E, 32.5°N 74.5°E), and over the megacity New
714 Delhi (radius of 25 km, or 50 km for CHOCHO) as observed with TROPOMI. The year 2020 is represented in red (2018
715 in blue, 2019 in black). With the HCHO and CHOCHO time series, the OMI climatology is shown for comparison (dashed
716 black line, 2010–2018), the error bars represent the interannual variability of the two-week averaged columns. The HCHO
717 columns have been corrected in order to assume the same temperature every year (see Sect. 2).

718

719 A large part of the observed HCHO and CHOCHO columns for India are due to natural emissions which can vary
720 significantly due to changes in meteorology, in particular temperature and precipitation. Hence a possible reduction
721 of the anthropogenic VOC emissions due to the lockdown measures is expected to have a small contribution to the
722 variability of the measured columns. During the most stringent phase 1 lockdown, a reduction in HCHO column
723 concentrations is observed for the IGP and is even more pronounced over New Delhi (Figure 9 top panels; respectively
724 -2 and -4×10^{15} molec cm^{-2} [-20% and -40%] compared to the OMI climatology for 2010–2018). In both cases, the
725 anomaly is larger than the interannual variations observed during this period (about 1.5×10^{15} molec cm^{-2}), where
726 changes in temperature or precipitation do not seem to explain the observed column decrease during phase 1. The



727 observed column decline is even more pronounced over New Delhi than over the IGP, suggesting that the origin of
728 the reduction is mostly anthropogenic.

729 The case for lockdown-driven reductions is further supported by the CHOCHO observations, which exhibit the
730 clearest COVID-19 signal during phase 1 of the lockdown (Figure 9). The reduction of CHOCHO during the lockdown
731 period over the IGP is slightly larger than the interannual variability of 1×10^{14} molec cm^{-2} (or -25%) as determined
732 from the OMI CHOCHO climatology. Similar to HCHO, the reduction in CHOCHO over New Delhi is twice as large
733 (-50%) and well beyond the 1-sigma OMI climatology range. Phase 2 is also characterized by lower CHOCHO column
734 amounts in 2020 as compared to 2019, but temperatures are also lower, unlike phase 1. Accounting for temperature-
735 driven variability (Sect. 2.5) brings the HCHO columns close to the mean HCHO seasonal levels. The somewhat more
736 pronounced effect of the lockdown on CHOCHO compared to HCHO in New Delhi is most likely due to the strong
737 contribution of anthropogenic VOC precursors to CHOCHO amounts (Chan Miller et al., 2016). Interestingly, fire
738 counts show that there were fewer fires in May 2020 compared to previous years (Fig. D2), most likely as a
739 consequence of the lockdown measures, which may also contribute to the lower glyoxal columns.

740 As it was the case for China, it is more difficult to identify a signal in CO column data driven by the COVID-19
741 lockdowns over India. An important reason for this is the much longer atmospheric residence time of CO that varies
742 depending on the OH concentration (Holloway et al., 2000). Moreover, according to bottom-up inventories, the major
743 anthropogenic CO source in India are due to the residential sector (42%), road transportation (21%), agricultural waste
744 burning (18%) and the industrial sector (16%) (Granier et al., 2019). Hence, during a lockdown we expect that the
745 main source of CO, residential, to be less affected. Figure 7 shows that the CO amounts in southern India are higher
746 in 2020 compared to 2019. The reason could be the accumulation of CO originating from elsewhere prior to the
747 lockdown period. The long atmospheric residence time of CO complicates the identification of COVID-19 lockdown
748 signals. Also for CO we derived the full TROPOMI time series for the IGP and New Delhi as shown in Figure 9
749 (lower panel). The time series for New Delhi in mid-April shows somewhat lower CO values in 2020 compared to
750 2019, but the large natural variability of CO prevents clear identification of a COVID-19 lockdown driven effect. In
751 future, analysis of a longer TROPOMI CO time series or model experiments may help to quantify the COVID-19
752 effects.

753

754 **6 Conclusions**

755 In this paper, we have analyzed the impact of COVID-19 lockdown measures on air quality around the globe, based
756 on observations of several trace gases from the Sentinel-5P/TROPOMI instrument. TROPOMI provides daily, global
757 observations of multiple trace gases, where the measured vertical column amounts are driven by emissions as well as
758 atmospheric and chemical processes of transport, transformation, and deposition. We compared the 2020 TROPOMI
759 data with similar periods from previous years and carried out additional analysis to disentangle changes in emissions
760 due to COVID-19 lockdown measures from meteorological variability, seasonal variability, and from other non-
761 lockdown emission drivers. We analyzed time series of NO_2 measurements from city to regional scales for several
762 locations around the globe, showing the potential of TROPOMI to globally monitor local to regional impacts of



763 COVID-19 lockdown measures on air quality and anthropogenic emissions. Furthermore, for the first time, we used
764 a combination of five trace gases observed by TROPOMI, specifically NO₂, SO₂, CO, HCHO and CHOCHO, to assess
765 the impact of COVID-19 related lockdown measures on trace gas concentrations.

766 From the global to city scale, we have illustrated consistent, sharp decreases in NO₂ concentrations driven by the
767 COVID-19-related lockdown measures. These findings are based on detailed analysis of the distribution of NO₂ using
768 daily measurements from TROPOMI. For the city of Wuhan in China, the first city to issue a lockdown, NO₂
769 concentrations measured by TROPOMI were about 60% lower than the same period in February-March 2019. After
770 China, lockdowns were issued across all continents and for the majority of countries from March through May 2020.
771 For megacities all over the world, reductions in column amounts of tropospheric NO₂ range between 14% and 63%.
772 The strength of the reduction depends on the type and efficiency of local measures carried out and on the relative
773 contribution of traffic, industry, and power generation to NO₂ emissions for a given area. Owing to the unprecedented
774 resolution of TROPOMI of about 5 km, reductions of different source contributions to NO₂ such as city traffic,
775 highways (Liu et al., 2020), power plants (Miyazaki et al., 2020), industry, and shipping (Ding et al., 2020) can be
776 estimated separately.

777 As demonstrated by time series analysis of the NO₂ observations, there is substantial variability even in two-week
778 averages, which is attributable to meteorological variability. On average, we estimate the standard deviation of this
779 variability to be about 13% (1-sigma standard deviation) for major cities in Europe, but locally the effect can
780 sometimes be larger. The large and systematic reductions (30-60%) observed, however, cannot be explained by
781 meteorological variability alone and are therefore attributed to the effect of the lockdown measures.

782 For SO₂, we observe significant column reductions in China and India over coal-fired power plants, which are the
783 primary sources of anthropogenic SO₂ in these areas. Over northeastern China in late February 2020, large reductions
784 of SO₂ vertical column amounts were observed, as a result of lockdown measures, with a decrease up to 77% as
785 compared to the same time period in 2019, which cannot be explained by interannual variability alone. An analysis of
786 SO₂ vertical column amounts over the largest SO₂-emitting power plants in India, reveals a reduction in SO₂ of about
787 25% during the first two phases of the lockdown, as compared to 2019. For India, the reductions in SO₂ were highly
788 correlated with NO₂ reductions for the same power plants and with the national energy demand for that period.

789 The natural variability of HCHO and CHOCHO does not allow detection of a significant decrease due to the COVID-
790 19 measures in most regions of the world based on TROPOMI observations alone. Exceptions are northern China and
791 New Delhi, where observed reductions could be attributed to the lockdown measures. For northeastern China, a 50%
792 reduction in the CHOCHO concentration is observed during the second half February, which is larger than the typical
793 observed interannual variability of 30%. For HCHO, after correcting for the effect of seasonal and temperature
794 variations, we observe a coincident 40%. We analyzed column amounts of CO, CHOCHO, and HCHO over the Indo-
795 Gangetic Plain, which is the most densely populated region of India. For CHOCHO and HCHO, we observed small
796 reductions in column amount due the COVID-19 measures, where these observed effects are slightly larger than the
797 interannual variability as determined using an OMI climatology (2010-2018). The observed reduction of 25% of
798 CHOCHO in this region is of the same order as the typical interannual variability. A stronger reduction of 60% is
799 observed for the city of New Delhi, which is similar to the reduction observed over northern China but occurs later



800 due to the difference in lockdown timing. For HCHO, we also observe a significant 40% decrease over New Delhi in
801 April, while over the whole Indo-Gangetic Plain, a decrease of 20% is observed.

802 For CO, reductions related to COVID-19 measures were much more difficult to identify, although over northern
803 China we see that the reductions in CO correlate with those for HCHO and CHOCHO. We could not find a similar
804 effect for CO over New Delhi. The fact that it is so hard to draw conclusions for CO based on the TROPOMI data
805 alone is due to the high variability in CO driven by meteorological conditions, in combination with the difficulty of
806 distinguishing localized emission changes from the high and variable background values, caused by the long
807 atmospheric lifetime of CO.

808 TROPOMI data have already been used in many publications (Gkatzelis et al., 2021; Bauwens et al., 2020; Liu et
809 al., 2020; Huang et al., 2020) aiming to analyze the impact of COVID-19 lockdown measures on air pollution levels.
810 Predominantly, these studies have been based on the use of TROPOMI NO₂ observations alone. We anticipate that
811 the combined use of multiple trace gases from TROPOMI together with the high spatial resolution of the
812 measurements, has large potential for a significantly improved sector-specific analysis of the impact of the COVID-
813 19 lockdown measures than previously possible. Such a multi-species analysis offers promise for in-depth
814 understanding of changes in air quality, the chemical interplay of pollutants in the atmosphere and their relation to
815 emissions. While keeping in mind the importance of accounting for interannual, seasonal, and meteorologically driven
816 variability (e.g. Miyazaki et al., 2020), it is clear that a detailed analysis cannot be based on TROPOMI observations
817 alone. For more quantitative estimates of the impact of COVID-19 lockdown measures on trace gas concentrations
818 and emissions, we need (inverse) models driven by high-quality meteorological analyses, or at least wind information
819 or statistical relationships to account for weather-driven variability (Goldberg et al., 2020; Miyazaki et al., 2020; Ding
820 et al., 2020).

821 In summary, our analyses using the most recent operational and scientific retrieval techniques have shown that by
822 taking emission sources, atmospheric lifetime as well the seasonal and meteorological variability into account for a
823 variety of trace gases measured by TROPOMI, rapid changes in anthropogenic emissions can be observed as induced
824 by the implementation of regional COVID-19 lockdown measures. It is our hope that this case study will serve as
825 reference for future analyses aimed at characterizing emission changes of not just NO₂, but by utilizing the
826 concomitant observation of the variety of trace gases measured by TROPOMI.

827

828 Appendix A

829 **Table A1: Summary of documentation available for TROPOMI operational data products from the Sentinel 5-P Library**
830 **(<https://sentinels.copernicus.eu/web/sentinel/technical-guides/sentinel-5p/products-algorithms>).**

Title	Document content description and product-specific reference	Document and Data links
Product Readme File (PRF)	Description of changes between different product versions and overall quality information	https://sentinels.copernicus.eu/web/sentinel/technical-guides/sentinel-5p/products-algorithms



	NO₂	Eskes and Eichmann, 2020	
	CO	Landgraf et al., 2020	
	HCHO	De Smedt et al., 2020a	
Product User Manual (PUM)		Technical description of file formatting for each TROPOMI Level 2 operational data product	https://sentinels.copernicus.eu/web/sentinel/technical-guides/sentinel-5p/products-algorithms
	NO₂	Eskes et al., 2020	
	CO	Apituley et al., 2018	
	HCHO	Romahn et al., 2020	
Algorithm Theoretical Basis Document (ATBD)		Detailed description of methods used for each TROPOMI L2 operational retrieval algorithm	https://sentinels.copernicus.eu/web/sentinel/technical-guides/sentinel-5p/products-algorithms
	NO₂	van Geffen et al., 2019	
	CO	Landgraf et al., 2018	
	HCHO	De Smedt et al., 2020b	
Quarterly Validation Report (ROCVR)		Detailed description of the latest validation available for each TROPOMI L2 operational dataset, product-specific	https://mpc-vdaf.tropomi.eu/
Operational Data Product Specifications		Product-specific overview pages with TROPOMI L2 dataset specifications, including how to access and how to cite each data product.	https://sentinels.copernicus.eu/web/sentinel/data-products
Operational Data Product Citation and Digital Object Identifier (DOI)	NO₂	Copernicus Sentinel 5-P, 2018a	doi:10.5270/S5P-s4ljg54
	CO	Copernicus Sentinel 5-P, 2018b	doi:10.5270/S5P-1hkp7rp
	HCHO	Copernicus Sentinel 5-P, 2018c	doi:10.5270/S5P-tjlxfd2

831

832 **Appendix B**

833 Appendix B contains additional information supporting the timing of COVID-19 driven emissions changes for global
 834 cities evaluated in this study and shown in Fig. 2.

835

836 **Table B2. Details about the lockdown dates for the cities illustrated in Figure 2.**



City	Date (2020)	Comment	Reference
Wuhan	23 January	Lockdown Wuhan and Hubei province	Bloomberg (2020)
	8 April	Lockdown lifted	Bloomberg (2020)
Mumbai and New Delhi	24 March	Closure of schools, public transport and most businesses	BBC (2020a)
	31 May	Nationwide lockdown is extended until end of May	Aljazeera (2020a)
Manila	16 March	Philippines announced strict home quarantine	Calonzo and Jiao (2020)
	1 June	Most businesses allowed to re-open, but bars, restaurants and schools remain closed	Jennings (2020)
Madrid	14 March	Nationwide lockdown	Minder and Peltier (2020)
	9 May	Easing, stores and restaurants allowed to open	Goodman et al. (2020)
Milan	8 March	Locking down of Northern Italy including Milan	Horowitz (2020a)
	4 May	Loosening of strictest lockdown measures	Horowitz (2020b)
Paris	17 March	France imposes nationwide the restriction	Onishi and Méheut (2020)
	11 May	Gradually relaxed lockdown measures, most shops open	Makooi (2020)
Los Angeles	19 March	California enters lockdown	BBC (2020b)
	1 June	Reopening of some shops and restaurants	Patel (2020)
New York	22 March	New York state enters lockdown	BBC (2020b)
	13 June	Stay-at-home orders put in place until further notice	CBS News (2020)
Sydney	24 March	Strict lockdown measures adopted in Australia	Wahlquist (2020)
	15 May	New South Wales eases lockdown restrictions	Sonali (2020)
Auckland	23 March	In New Zealand stay-at-home orders are issued	Menon (2020)
	14 May	All businesses can open in New Zealand	Conforti (2020)
Mexico City	23 March	Most economic sectors stopped in Mexico	Pasley (2020)
	1 June	Gradual reopening of Mexico city	Associated Press (2020)
Lima	16 March	Stringent quarantine enforced by police and army	Collyns (2020)



	30 June	Peru extended nationwide lockdown through end of June	Aljazeera (2020b)
Sao Paulo	24 March	Start of lockdown, but measures were largely ignored	Uchoa (2020)
	31 May	Quarantine extended through May	CGTN (2020)
Buenos Aires	20 March	Argentina under mandatory lockdown	Do Rosario and Gillespie (2020)
	28 June	Lockdown extended	Misculin and Garrison (2020)
Baghdad	22 March	Iraq imposed a total nationwide lockdown	The Star (2020)
	21 April	Relaxed restrictions: shops reopen for limited hours	Saleh (2020)
	20 May	In Baghdad strict lockdown re-imposed for 6 districts	Saleh (2020)
Lagos	30 March	Stay-at-home order, markets open for limited hours	Orjinmo (2020)
	4 May	Easing of restrictions, but schools, bars, and cinemas remain closed	Mbah (2020)
Johannesburg	26 March	Stay-at-home orders issued in South Africa	Winter (2020)
	1 June	Most economic sectors permitted to operate	Aljazeera (2020c)

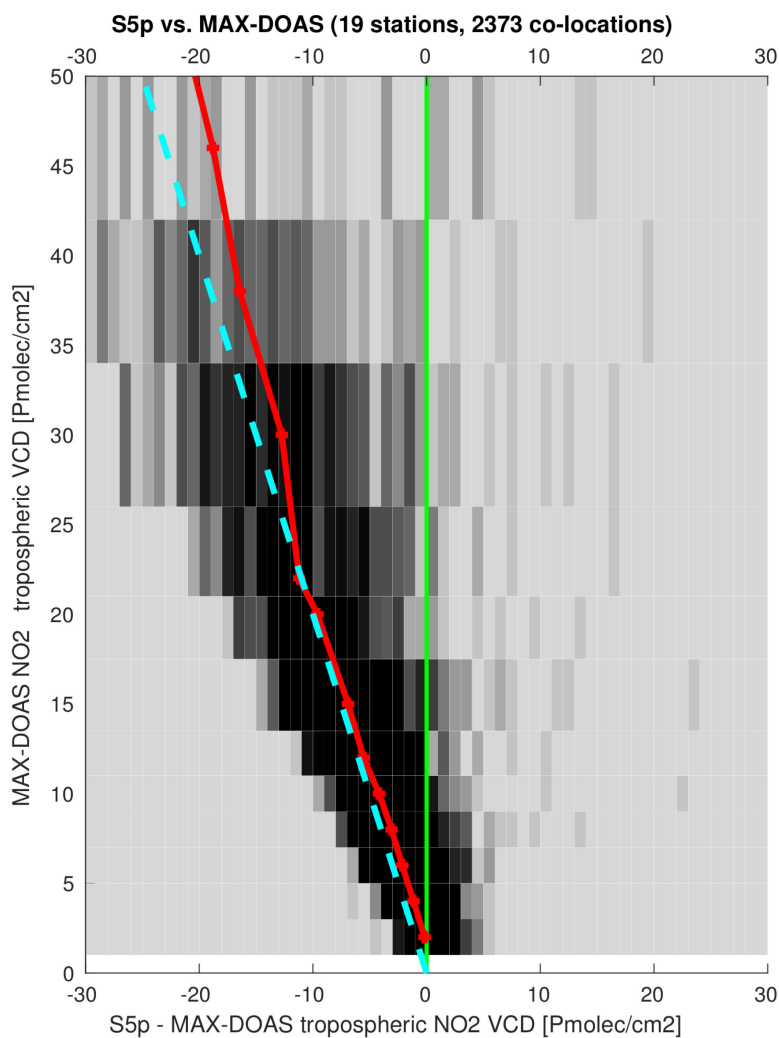
837

838

839 **Appendix C**

840 Appendix C contains figures which support the technical understanding of individual retrieval algorithms.

841



842

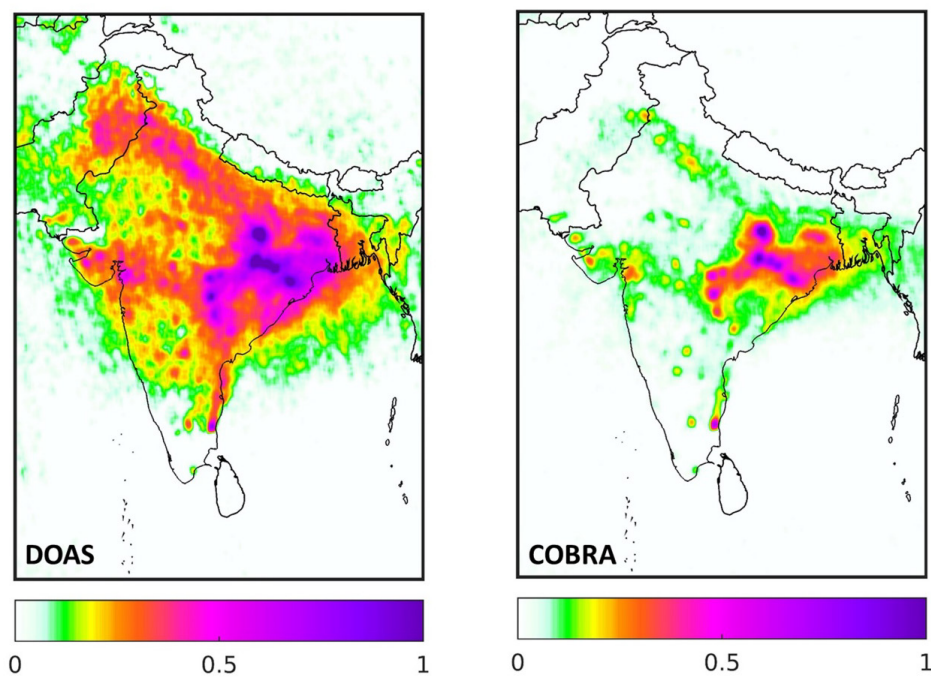
843 **Figure C1: Bias in S5p-TROPOMI tropospheric NO₂ as estimated from comparisons to co-located ground-based MAX-**
844 **DOAS measurements, presented as a function of the ground-based VCD measurement. The grey-scale background**
845 **represents a 2-D histogram, where the median difference per MAX-DOAS VCD bin is shown as the red curve, and the blue**
846 **dashed line shows a multiplicative bias (b) model with $b \sim 0.5 \times \text{VCD}$. More details on the ground-based data and**
847 **co-location scheme can be found in Verhoelst et al., 2021.**

848

849



SO₂ vertical column (DU) - April 2019

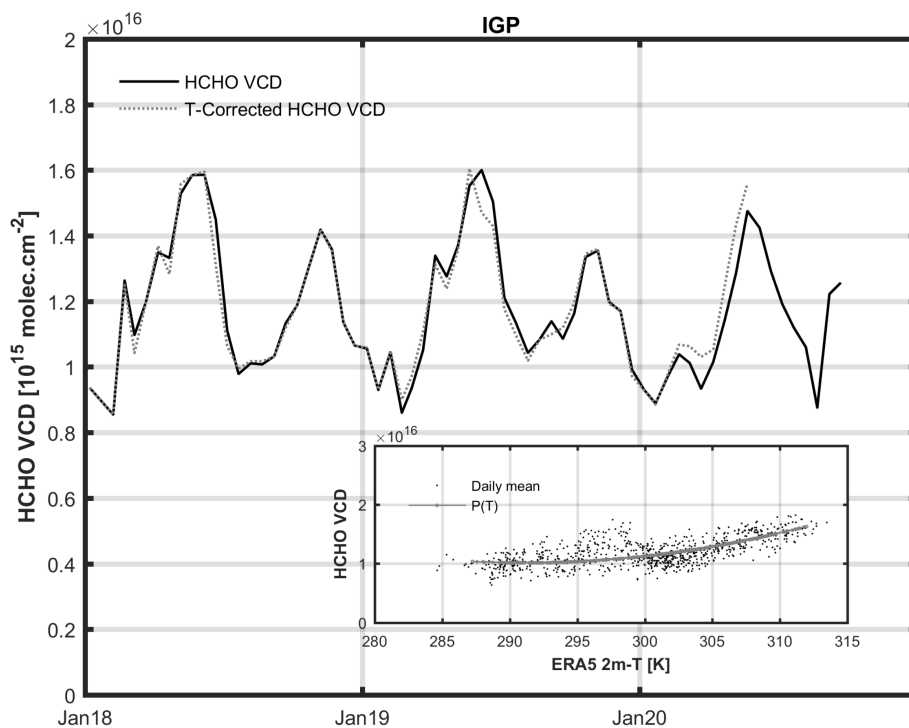


850

851 **Figure C2: Monthly averaged TROPOMI SO₂ columns over India for April 2019, from (left) DOAS operational product**
852 **and (right) COBRA scientific product. The noise and offsets reduction is clear from the maps. The emissions from individual**
853 **point sources (power plants) can be better discerned in the COBRA SO₂ map.**

854

855

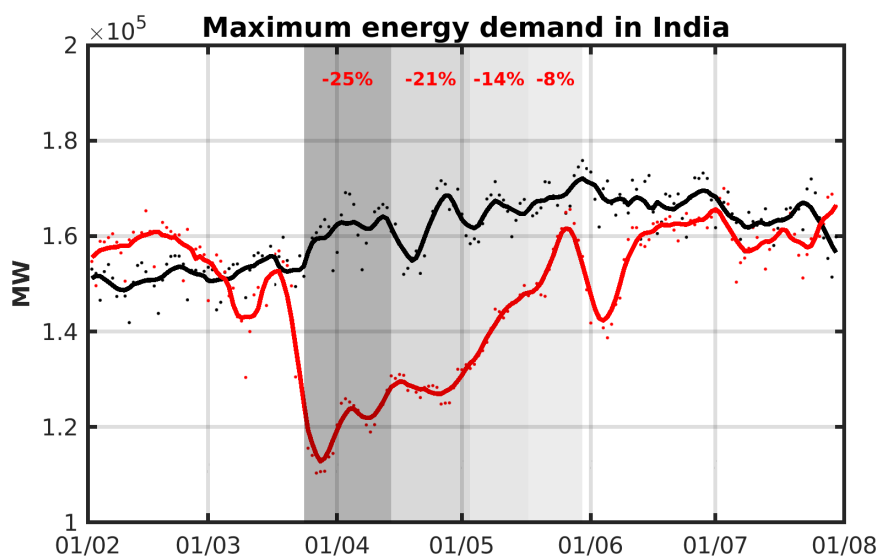


856

857 **Figure C3:** Example of temperature correction of the TROPOMI HCHO tropospheric columns in the Indogangetic Plain
858 region. The dashed line presents the HCHO columns after correction using climatological temperatures. The correlation
859 between the local daily temperatures from ERA5-Land 2m and the HCHO columns is shown inset for the entire period.

860 **Appendix D**

861 Appendix D contains additional figures that support the interpretation timing of observed changes in COVID-19
862 driven emissions related to power generation (Fig. D1) and meteorological conditions (Fig. D2).



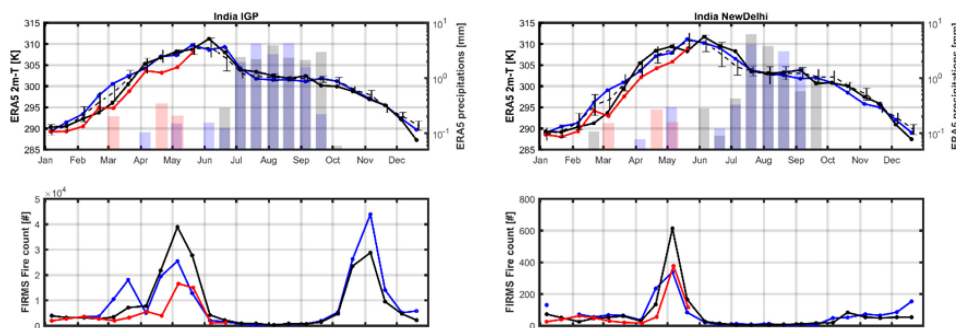
863

864 **Figure D1: Maximum energy demand over India during the period of the lockdown (red) compared to the same period in**
 865 **2019 (black), For each of the phases of the lockdown the reductions in maximum energy demand is given relative to the**
 866 **same period in 2019. Data from: www.posoco.in/covid-19.**

867

868

869



878 **Figure D2: Upper panels: ombrothermic diagrams for the same regions as shown in Figure 9 showing the two-week**
 879 **average temperature at 2m (upper left) and precipitation amounts (upper right, source ERA5, Muñoz Sabater, 2019b).**
 880 **Lower panels: fire counts (source FIRMS, <https://earthdata.nasa.gov/firms>). The year 2020 is represented in red, 2019 in**
 881 **black, and 2018 in blue.**

882



883 **Data Availability**

884 Operational versions of all Copernicus Sentinel 5-P Data TROPOMI data are freely available from the European
885 Union/ESA/Copernicus Sentinel-5P Pre-Operations Data Hub (<https://s5phub.copernicus.eu>; S5P Pre-Ops Data Hub,
886 2021). The TROPOMI COBRA SO₂ dataset is available on request as described in Theys et al., 2021. OMI HCHO
887 and NO₂ datasets are openly available on <http://www.qa4ecv.eu/ecvs>. TROPOMI Glyoxal data is available upon
888 request as a part of the ESA S5p+I GLYRETRO project as detailed on the project website:
889 <https://glyretro.aeronomie.be/>.

890 **Author Contributions**

891 PFL conceptualized, initiated, and managed this manuscript with contributions from IA, MB, TB, IDS, HE, CL, TS,
892 DSZ, NT, MVR, PV, and TV. Formal analysis was carried out by MB, TB, IDS, HE, CL, and NT. DL and FR provided
893 data curation and software support for TROPOMI HCHO data products. DSZ prepared, edited, and co-managed the
894 manuscript with contributions from IA, MB, TB, IDS, HE, CL, PFL, TS, NT, MVR, PV, and TV.

895 **Competing Interests**

896 The authors declare that they have no conflict of interest.

897 **Acknowledgements**

898 We acknowledge financial support from the following projects: ESA S5P MPC (4000117151/16/I-LG); Netherlands
899 Space Office TROPOMI Science Project; ESA S5p+Innovation GLYRETRO and ICOVAC projects (No.
900 4000127610/19/I-NS); Belgium Prodex TRACE-S5P (PEA 4000105598), and TROVA-2 (PEA 4000130630);
901 Belgium BRAIN-2.be LEGO-BEL-AQ; EU FP7 QA4ECV project (grant no. 607405). This paper contains modified
902 Copernicus data (2018/2020) processed by KNMI, BIRA-IASB, DLR, and SRON.

903 **References**

904 van der A, R., Mijling, B., Ding, J., Koukouli, M., Liu, F., Li, Q., Mao, H., and Theys, N.: Cleaning up the air:
905 Effectiveness of air quality policy for SO₂ and NO_x emissions in China, *Atmos. Chem. Phys.*, 17, 1775-1789,
906 doi:10.5194/acp-17-1775-2017, 2017.

907

908 Adigun, B. and Anna, C.: Nigeria confirms 1st case of new virus in sub-Saharan Africa, AP News,
909 <https://apnews.com/article/5de56b2fc9fae583c7c57b82c1a4fff>, last access: 30 March 2021, 2020.

910



- 911 Aljazeera: Coronavirus in India: What we know about world's largest lockdown,
912 <https://www.aljazeera.com/news/2020/05/india-coronavirus-crisis-200519120521747.html>, last access: 17 June 2020,
913 2020a.
- 914
- 915 Aljazeera: Peru extends nationwide lockdown until end of June, <https://www.aljazeera.com/news/2020/05/peru-extends-nationwide-lockdown-june-200523073017946.html>, last access: 17 June 2020, 2020b.
- 916
- 917
- 918 Aljazeera: South Africa coronavirus lockdown to ease from June 1,
919 <https://www.aljazeera.com/news/2020/05/ramaphosa-south-africa-coronavirus-lockdown-ease-june-1-200525070634938.html>, last access: 17 June 2020, 2020c.
- 920
- 921
- 922 Aloi, A., Alonso, B., Benavente, J., Cordera, R., Echániz, E., González, F., Ladisa, C., Lezama-Romanelli, R., López-
923 Parra, Á., Mazzei, V., Perrucci, L., Prieto-Quintana, D., Rodríguez, A. and Sañudo, R.: Effects of the COVID-19
924 Lockdown on Urban Mobility: Empirical Evidence from the City of Santander (Spain), *Sustainability*, 12(9), 3870,
925 doi:10.3390/su12093870, 2020.
- 926
- 927 Alvarado, L., Richter, A., and Lerot, C.: GLYoxal Retrievals from TROPOMI (GLYRETRO) Validation Report,
928 S5p+Innovation – theme 1 (CHOCHO), 5p+I_CHOCHO_BIRA_VR, 1.1, 35 pp., <https://glyretro.aeronomie.be/>,
929 2020.
- 930
- 931 Apituley, A., Pedergrana, M., Sneep, M., Veeffkind, J. P., Loyola, D., Landgraf, J., and Borsdorff, T.: Sentinel-5
932 precursor/TROPOMI Level 2 Product User Manual Carbon Monoxide, document number: SRON-S5P-LEV2-MA-
933 002, 1.0.0, SRON Netherlands Institute for Space Research, Utrecht, The Netherlands,
934 <https://sentinels.copernicus.eu/web/sentinel/technical-guides/sentinel-5p/products-algorithms>, 2018.
- 935
- 936 Associated Press: Mexico City will begin gradually reopening June 1, mayor says, <https://www.latimes.com/world-nation/story/2020-05-21/mexico-city-will-begin-gradual-reopening-coronavirus-june-1>, last access: 17 June 2020,
937 2020.
- 938
- 939
- 940 Baldasano, J. M.: COVID-19 lockdown effects on air quality by NO₂ in the cities of Barcelona and Madrid (Spain),
941 *Sci. Total Environ.*, 741, 140353, doi:10.1016/j.scitotenv.2020.140353, 2020.
- 942
- 943 Barré, J., Petetin, H., Colette, A., Guevara, M., Peuch, V.-H., Rouil, L., Engelen, R., Inness, A., Flemming, J., Pérez
944 García-Pando, C., Bowdalo, D., Meleux, F., Geels, C., Christensen, J. H., Gauss, M., Benedictow, A., Tsyro, S., Friese,
945 E., Struzewska, J., Kaminski, J. W., Douros, J., Timmermans, R., Robertson, L., Adani, M., Jorba, O., Joly, M., and
946 Kouznetsov, R.: Estimating lockdown-induced European NO₂ changes using satellite and surface observations and air
947 quality models, *Atmos. Chem. Phys.*, 21, 7373–7394, doi:10.5194/acp-21-7373-2021, 2021.



948
949 Bauwens, M., Stavrou, T., Müller, J.-F., De Smedt, I., Van Roozendaal, M., van der Werf, G. R., Wiedinmyer, C.,
950 Kaiser, J. W., Sindelarova, K. and Guenther, A.: Nine years of global hydrocarbon emissions based on source inversion
951 of OMI formaldehyde observations, *Atmos. Chem. Phys.*, 16(15), 10133–10158, doi:10.5194/acp-16-10133-2016,
952 2016.
953
954 Bauwens, M. Compernelle, S., Stavrou, T., Müller, J.-F., van Gent, J., Eskes, H., Levelt, P. F., van der A, R.,
955 Veeffkind, J. P., Vlietinck, J., Yu, H., and Zehner, C.: Impact of coronavirus outbreak on NO₂ pollution assessed using
956 TROPOMI and OMI observations, *Geophys. Res. Lett.*, 47(11), doi:10.1029/2020GL087978, 2020.
957
958 BBC: India extends coronavirus lockdown by two weeks, <https://www.bbc.com/news/world-asia-india-52698828>, last
959 access: 17 June 2020, 2020a.
960
961 BBC: Earlier coronavirus lockdown 'could have saved 36,000 lives', [https://www.bbc.com/news/world-us-canada-](https://www.bbc.com/news/world-us-canada-52757150)
962 [52757150](https://www.bbc.com/news/world-us-canada-52757150), last access: 17 June 2020, 2020b.
963
964 Beirle, S., Borger, C., Dörner, S., Li, A., Hu, Z., Liu, F., Wang, Y., and Wagner, T.: Pinpointing nitrogen oxide
965 emissions from space, *Sci. Adv.* 5, doi:10.1126/sciadv.aax9800, 2019.
966
967 Beirle, S., Borger, C., Dörner, S., Eskes, H., Kumar, V., de Laat, A., and Wagner, T.: Catalog of NO_x emissions from
968 point sources as derived from the divergence of the NO₂ flux for TROPOMI, *Earth Syst. Sci. Data Discuss.* [preprint],
969 doi:10.5194/essd-2020-280, in review, 2021.
970
971 Bloomberg News: China to lift lockdown over virus epicenter Wuhan on April 8,
972 [https://www.bloomberg.com/news/articles/2020-03-24/china-to-lift-lockdown-over-virus-epicenter-wuhan-on-april-](https://www.bloomberg.com/news/articles/2020-03-24/china-to-lift-lockdown-over-virus-epicenter-wuhan-on-april-8)
973 [8](https://www.bloomberg.com/news/articles/2020-03-24/china-to-lift-lockdown-over-virus-epicenter-wuhan-on-april-8), last access: 1 July 2020, 2020.
974
975 Boersma, K. F., Eskes, H. J., Richter, A., De Smedt, I., Lorente, A., Beirle, S., van Geffen, J. H. G. M., Zara, M.,
976 Peters, E., Van Roozendaal, M., Wagner, T., Maasackers, J. D., van der A, R. J., Nightingale, J., De Rudder, A., Irie,
977 H., Pinardi, G., Lambert, J.-C., and Compernelle, S.: Improving algorithms and uncertainty estimates for satellite NO₂
978 retrievals: Results from the Quality Assurance for Essential Climate Variables (QA4ECV) project, *Atmos. Meas.*
979 *Tech.*, 11, 6651-6678, doi:10.5194/amt-11-6651-2018, 2018.
980
981 Borsdorff, T., Hasekamp, O. P., Wassmann, A., and Landgraf, J.: Insights into Tikhonov regularization: Application
982 to trace gas column retrieval and the efficient calculation of total column averaging kernels, *Atmos. Meas. Tech.*, 7(2),
983 523–535, 2014.
984



- 985 Borsdorff, T., Tol, P., Williams, J. E., de Laat, J., aan de Brugh, J., Nédélec, P., Aben, I., and Landgraf, J.: Carbon
986 monoxide total columns from SCIAMACHY 2.3 μm atmospheric reflectance measurements: towards a full-mission
987 data product (2003–2012), *Atmos. Meas. Tech.*, 9, 227–248, doi:10.5194/amt-9-227-2016, 2016.
- 988
- 989 Borsdorff, T., aan de Brugh, J., Hu, H., Nédélec, P., Aben, I., and Landgraf, J.: Carbon monoxide column retrieval for
990 clear-sky and cloudy atmospheres: a full-mission data set from SCIAMACHY 2.3 μm reflectance measurements,
991 *Atmos. Meas. Tech.*, 10, 1769–1782, doi:10.5194/amt-10-1769-2017, 2017.
- 992
- 993 Borsdorff, T., aan de Brugh, J., Hu, H., Hasekamp, O., Sussmann, R., Rettinger, M., Hase, F., Gross, J., Schneider,
994 M., Garcia, O., Stremme, W., Grutter, M., Feist, D. G., Arnold, S. G., De Mazière, M., Kumar Sha, M., Pollard, D.
995 F., Kiel, M., Roehl, C., Wennberg, P. O., Toon, G. C., and Landgraf, J.: Mapping carbon monoxide pollution from
996 space down to city scales with daily global coverage, *Atmos. Meas. Tech.*, 11, 5507–5518, doi:10.5194/amt-11-5507-
997 2018, 2018.
- 998
- 999 Borsdorff, T., aan de Brugh, J., Pandey, S., Hasekamp, O., Aben, I., Houweling, S., and Landgraf, J.: Carbon monoxide
1000 air pollution on sub-city scales and along arterial roads detected by the Tropospheric Monitoring Instrument, *Atmos.*
1001 *Chem. Phys.*, 19, 3579–3588, doi:10.5194/acp-19-3579-2019, 2019.
- 1002
- 1003 Borsdorff, T., García Reynoso, A., Maldonado, G., Mar-Morales, B., Stremme, W., Grutter, M., and Landgraf, J.:
1004 Monitoring CO emissions of the metropolis Mexico City using TROPOMI CO observations, *Atmos. Chem. Phys.*,
1005 20, 15761–15774, doi:10.5194/acp-20-15761-2020, 2020.
- 1006
- 1007 Bovensmann, H., Burrows, J. P., Buchwitz, M., Frerick, J., Noel, S., Rozanov, V. V., Chance, L.V., and Goede,
1008 A.P.H.: SCIAMACHY: Mission objectives and measurement modes, *Atmos. Sci.*, 56, 127-150, 1999.
- 1009
- 1010 Braaten, J.: Monitoring air quality with S5P TROPOMI data, Medium, [https://medium.com/google-earth/monitoring-](https://medium.com/google-earth/monitoring-air-quality-with-s5p-tropomi-data-4f6b0aeb1c0)
1011 [air-quality-with-s5p-tropomi-data-4f6b0aeb1c0](https://medium.com/google-earth/monitoring-air-quality-with-s5p-tropomi-data-4f6b0aeb1c0), last access: 20 June 2021, 2020.
- 1012
- 1013 Broomandi, P., Karaca, F., Nikfal, A., Jahanbakhshi, A., Tamjidi, M., and Kim, J. R.: Impact of COVID-19 Event on
1014 the Air Quality in Iran. *Aerosol Air Qual. Res.*, 20, 1793–1804, doi:10.4209/aaqr.2020.05.0205, 2020.
- 1015
- 1016 Calonzo, A. and Jiao C.: Duterte expands Philippine lockdown to 60 million people,
1017 [https://www.bloomberg.com/news/articles/2020-03-16/duterte-widens-lockdown-to-main-philippine-island-to-fight-](https://www.bloomberg.com/news/articles/2020-03-16/duterte-widens-lockdown-to-main-philippine-island-to-fight-virus)
1018 [virus](https://www.bloomberg.com/news/articles/2020-03-16/duterte-widens-lockdown-to-main-philippine-island-to-fight-virus), last access: 17 June 2020, 2020a.
- 1019
- 1020 Cao, H., Fu, T.-M., Zhang, L., Henze, D. K., Miller, C. C., Lerot, C., Abad, G. G., De Smedt, I., Zhang, Q., van
1021 Roozendaal, M., Hendrick, F., Chance, K., Li, J., Zheng, J. and Zhao, Y.: Adjoint inversion of Chinese non-methane



- 1022 volatile organic compound emissions using space-based observations of formaldehyde and glyoxal, *Atmos. Chem.*
1023 *Phys.*, 18(20), 15017–15046, doi:10.5194/acp-18-15017-2018, 2018.
- 1024
- 1025 CBS News: Lockdown extended for most of coronavirus-battered New York, [https://www.cbsnews.com/news/new-](https://www.cbsnews.com/news/new-york-stay-at-home-extended-coronavirus-lockdown/)
1026 [york-stay-at-home-extended-coronavirus-lockdown/](https://www.cbsnews.com/news/new-york-stay-at-home-extended-coronavirus-lockdown/), last access: 17 June 2020, 2020.
- 1027
- 1028 CGTN: Sao Paulo extends the quarantine through May, [https://newsus.cgtn.com/news/2020-05-10/Sao-Paulo-](https://newsus.cgtn.com/news/2020-05-10/Sao-Paulo-extends-quarantine-through-May-QmDnOJo6bK/index.html)
1029 [extends-quarantine-through-May-QmDnOJo6bK/index.html](https://newsus.cgtn.com/news/2020-05-10/Sao-Paulo-extends-quarantine-through-May-QmDnOJo6bK/index.html), last access: 1 July 2020, 2020.
- 1030
- 1031 Chan Miller, C., Jacob, D. J., González Abad, G., and Chance, K.: Hotspot of glyoxal over the Pearl River delta seen
1032 from the OMI satellite instrument: implications for emissions of aromatic hydrocarbons, *Atmos. Chem. Phys.*, 16,
1033 4631–4639, doi:10.5194/acp-16-4631-2016, 2016.
- 1034
- 1035 Chang, Y., Huang, R.J., Ge, X., Huang, X., Hu, J., Duan, Y., Zou, Z., Liu, X., and Lehmann, M. F.: Puzzling haze
1036 events in China during the coronavirus (COVID-19) shutdown. *Geophys. Res. Lett.*, 47, e2020GL088533,
1037 doi:10.1029/2020GL088533, 2020.
- 1038
- 1039 Collivignarelli, M. C., Abba, A., Bertanza, G., Pedrazzani, R., Ricciardi, P., and Miino, M. C.: Lockdown for Covid-
1040 2019 in Milan: What are the effects on air quality?, *Sci. Total Environ.*, 732, 139280,
1041 doi:10.1016/j.scitotenv.2020.139280, 2020.
- 1042
- 1043 Collins, D.: Peru’s coronavirus response was ‘right on time’ – so why isn’t it working?, *The Guardian*,
1044 <https://www.theguardian.com/global-development/2020/may/20/peru-coronavirus-lockdown-new-cases>, last access:
1045 17 June 2020, 2020.
- 1046
- 1047 Conforti K.: Alert Level 2 restrictions to begin in New Zealand this week,
1048 [https://www.forbes.com/sites/kaeliconforti/2020/05/13/alert-level-2-restrictions-to-begin-in-new-zealand-this-](https://www.forbes.com/sites/kaeliconforti/2020/05/13/alert-level-2-restrictions-to-begin-in-new-zealand-this-week/#52517b326497)
1049 [week/#52517b326497](https://www.forbes.com/sites/kaeliconforti/2020/05/13/alert-level-2-restrictions-to-begin-in-new-zealand-this-week/#52517b326497), last access: 17 June 2020, 2020.
- 1050
- 1051 Copernicus Sentinel-5P (processed by ESA): TROPOMI Level 2 Nitrogen Dioxide total column products. Version
1052 01. European Space Agency, doi:10.5270/S5P-s4ljg54, 2018a.
- 1053
- 1054 Copernicus Sentinel-5P (processed by ESA): TROPOMI Level 2 Carbon Monoxide total column products. Version
1055 01. European Space Agency, doi:10.5270/S5P-1hkp7rp, 2018b.
- 1056
- 1057 Copernicus Sentinel-5P (processed by ESA): TROPOMI Level 2 Formaldehyde Total Column products. Version 01.
1058 European Space Agency, doi:10.5270/S5P-tjlxfd2, 2018c.



- 1059
- 1060 Dattakiran, J.: Impact of lockdown on India's electricity sector, EnergyA, <http://www.energy-a.eu/impact-of-ongoing->
1061 [lockdown-on-indias-electricity-sector-an-overview/](http://www.energy-a.eu/impact-of-ongoing-lockdown-on-indias-electricity-sector-an-overview/), last access: 9 June 2020, 2020.
- 1062
- 1063 De Smedt, I., Theys, N., Yu, H., Danckaert, T., Lerot, C., Compennolle, S., Van Roozendael, M., Richter, A., Hilboll,
1064 A., Peters, E., Pedernana, M., Loyola, D., Beirle, S., Wagner, T., Eskes, H., van Geffen, J., Boersma, K. F., and
1065 Veefkind, P.: Algorithm theoretical baseline for formaldehyde retrievals from S5P TROPOMI and from the QA4ECV
1066 project, Atmos. Meas. Tech., 11, 2395–2426, doi:10.5194/amt-11-2395-2018, 2018.
- 1067
- 1068 De Smedt, I., Romahn, F., and Eichmann, K.-U.: S5P Mission Performance Centre Formaldehyde [L2_HCHO_]
1069 Readme, document number: S5P-MPC-BIRA-PRF-HCHO, 2.1, BIRA-IASB Royal Belgian Institute for Space
1070 Aeronomy, Brussels, Belgium, <https://sentinels.copernicus.eu/web/sentinel/technical-guides/sentinel-5p/products->
1071 [algorithms](https://sentinels.copernicus.eu/web/sentinel/technical-guides/sentinel-5p/products-algorithms), 2020a.
- 1072
- 1073 De Smedt, I., Theys, N., Yu, H., Vlietinck, J., Lerot, C., and Van Roozendael, M.: S5P/TROPOMI HCHO ATBD,
1074 document number: S5P-BIRA-L2-400F-ATBD, 2.2.0, BIRA-IASB Royal Belgian Institute for Space Aeronomy,
1075 Brussels, Belgium, <https://sentinels.copernicus.eu/web/sentinel/technical-guides/sentinel-5p/products-algorithms>,
1076 2020b.
- 1077
- 1078 Diamond, M. S. and Wood, R.: Limited regional aerosol and cloud microphysical changes despite unprecedented
1079 decline in nitrogen oxide pollution during the February 2020 COVID-19 shutdown in China, Geophys. Res. Lett., 47,
1080 doi:10.1029/2020GL088913, 2020.
- 1081
- 1082 Dimitropoulou, E., Hendrick, F., Pinardi, G., Friedrich, M. M., Merlaud, A., Tack, F., De Longueville, H., Fayt, C.,
1083 Hermans, C., Laffineur, Q., Fierens, F., and Van Roozendael, M.: Validation of TROPOMI tropospheric NO₂ columns
1084 using dual-scan multi-axis differential optical absorption spectroscopy (MAX-DOAS) measurements in Uccle,
1085 Brussels, Atmos. Meas. Tech., 13, 5165–5191, doi:10.5194/amt-13-5165-2020, 2020.
- 1086
- 1087 Ding, J., van der A, R. J., Eskes, H. J., Mijling, B., Stavrou, T., van Geffen, J. H. G. M., and Veefkind, J. P.: NO_x
1088 emissions reduction and rebound in China due to the COVID-19 crisis. Geophys. Res. Lett., 46, e2020GL089912,
1089 doi.org:10.1029/2020GL089912, 2020.
- 1090
- 1091 Do Rosario, J., Gillespie P.: Argentina orders 'exceptional' Lockdown in bid to stem virus,
1092 <https://www.bloomberg.com/news/articles/2020-03-20/argentina-orders-exceptional-lockdown-in-bid-to-contain->
1093 [virus](https://www.bloomberg.com/news/articles/2020-03-20/argentina-orders-exceptional-lockdown-in-bid-to-contain-virus), last access: 17 June 2020, 2020.
- 1094
- 1095 Sentinel-5P Pre-Operations Data Hub: <https://s5phub.copernicus.eu/>, last access: 18 June 2021.



- 1096
1097 Eskes, H. J. and Boersma, K. F.: Averaging kernels for DOAS total-column satellite retrievals, *Atmos. Chem. Phys.*,
1098 3, 1285–1291, doi:10.5194/acp-3-1285-2003, 2003.
- 1099
1100 Eskes, H., van Geffen, J., Boersma, K. F., Eichmann, K.-U., Apituley, A., Pedernana, M., Sneep, M., Veeffkind, J.
1101 P., and Loyola, D.: Sentinel-5 precursor/TROPOMI Level 2 Product User Manual Nitrogen dioxide, document
1102 number: S5P-KNMI-L2-0021-MA, 4.0.0, Royal Netherlands Meteorological Institute, De Bilt, The Netherlands,
1103 <https://sentinels.copernicus.eu/web/sentinel/technical-guides/sentinel-5p/products-algorithms>, 2020.
- 1104
1105 Eskes, H. J., and Eichmann, K.-U.: S5P Mission Performance Centre Nitrogen Dioxide [L2_NO2_] Readme,
1106 document number: S5P-MPC-KNMI-PRF-NO2, 1.6, Royal Netherlands Meteorological Institute, De Bilt, The
1107 Netherlands, <https://sentinels.copernicus.eu/web/sentinel/technical-guides/sentinel-5p/products-algorithms>, 2020.
- 1108
1109 Forster, P. M., Forster, H. I., Evans, M. J., Gidden, M. J., Jones, C. D., Keller, C. A., Lamboll, R. D., Le Quéré, C.,
1110 Rogelj, J., Rosen, D., Schuessler, C.-F., Richardson, T. B., Smith, C. J., and Turnock, S. T.: Current and future global
1111 climate impacts resulting from COVID-19, *Nat. Clim. Chang.*, 10, 913–919, doi:10.1038/s41558-020-0883-0, 2020.
- 1112
1113 Fioletov, V. E., McLinden, C. A., Krotkov, N., Li, C., Joiner, J., Theys, N., Carn, S., and Moran, M. D.: A global
1114 catalogue of large SO₂ sources and emissions derived from the Ozone Monitoring Instrument, *Atmos. Chem. Phys.*,
1115 16, 11497–11519, doi:10.5194/acp-16-11497-2016, 2016.
- 1116
1117 Fioletov, V., McLinden, C. A., Griffin, D., Theys, N., Loyola, D. G., Hedelt, P., Krotkov, N. A., and Li, C.:
1118 Anthropogenic and volcanic point source SO₂ emissions derived from TROPOMI on board Sentinel-5 Precursor: first
1119 results, *Atmos. Chem. Phys.*, 20, 5591–5607, doi:10.5194/acp-20-5591-2020, 2020.
- 1120
1121 Fu, T.-M., Jacob, D. J., Wittrock, F., Burrows, J. P., Vrekoussis, M., and Henze, D. K.: Global budgets of atmospheric
1122 glyoxal and methylglyoxal, and implications for formation of secondary organic aerosols, *J. Geophys. Res.*, 113,
1123 D15303, doi:10.1029/2007JD009505, 2008.
- 1124
1125 van Geffen, J. H. G. M., Eskes, H. J., Boersma, K. F., Maasakkers, J. D., and Veeffkind, J. P.: TROPOMI ATBD of
1126 the total and tropospheric NO₂ data products, document number: S5P-KNMI-L2-0005-RP, 1.4.0, Royal Netherlands
1127 Meteorological Institute, De Bilt, The Netherlands, [https://sentinels.copernicus.eu/web/sentinel/technical-](https://sentinels.copernicus.eu/web/sentinel/technical-guides/sentinel-5p/products-algorithms)
1128 [guides/sentinel-5p/products-algorithms](https://sentinels.copernicus.eu/web/sentinel/technical-guides/sentinel-5p/products-algorithms), 2019.
- 1129
1130 van Geffen, J., Boersma, K. F., Eskes, H., Sneep, M., ter Linden, M., Zara, M., and Veeffkind, J. P.: S5P TROPOMI
1131 NO₂ slant column retrieval: method, stability, uncertainties and comparisons with OMI, *Atmos. Meas. Tech.*, 13,
1132 1315–1335, doi:10.5194/amt-13-1315-2020, 2020.



1133
1134 Gkatzelis, G. I., Gilman, J. B., Brown, S. S., Eskes, H., Gomes, A. R., Lange, A. C., McDonald, B. C., Peischl, J.,
1135 Petzold, A., Thompson, C. R., and Kiendler-Scharr, A.: The Global Impacts of COVID-19 Lockdowns on Urban Air
1136 Quality: A Critical Review and Recommendations, *Elem. Sci. Anth.*, 9, doi:10.1525/elementa.2021.00176, 2021.
1137
1138 Goldberg, D. L., Anenberg, S. C., Griffin, D., McLinden, C. A., Lu, Z., and Streets, D. G.: Disentangling the impact
1139 of the COVID-19 lockdowns on urban NO₂ from natural variability, *Geophys. Res. Lett.*, 47, e2020GL089269,
1140 doi:10.1029/2020GL089269, 2020.
1141
1142 Goodman, A.: De Moura H., and Rebaza C. After 7 weeks of lockdown, Spaniards can finally exercise outdoors --
1143 as death toll passes 25,000, [https://edition.cnn.com/2020/05/02/europe/spain-lockdown-coronavirus-exercise-](https://edition.cnn.com/2020/05/02/europe/spain-lockdown-coronavirus-exercise-intl/index.html)
1144 [intl/index.html](https://edition.cnn.com/2020/05/02/europe/spain-lockdown-coronavirus-exercise-intl/index.html), last access: 17 June 2020, 2020.
1145
1146 Granier, C., Darras, S., Denier van der Gon, H., Doubalova, J., Elguindi, N., Galle, B., Gauss, M., Guevara, M.,
1147 Jalkanen, J.-P., Kuenen, J., Liousse, C., Quack, B., Simpson, D., and Sindelarova, K.: The Copernicus Atmosphere
1148 Monitoring Service global and regional emissions (April 2019 version), Copernicus Atmosphere Monitoring Service
1149 (CAMS) Report, Laboratoire d'Aérodologie, Toulouse, France, 54pp., doi:10.24380/d0bn-kx16, 2019.
1150
1151 Guevara, M., Jorba, O., Soret, A., Petetin, H., Bowdalo, D., Serradell, K., Tena, C., Denier van der Gon, H., Kuenen,
1152 J., Peuch, V.-H., and Pérez García-Pando, C.: Time-resolved emission reductions for atmospheric chemistry modelling
1153 in Europe during the COVID-19 lockdowns, *Atmos. Chem. Phys.*, 21, 773–797, [https://doi.org/10.5194/acp-21-773-](https://doi.org/10.5194/acp-21-773-2021)
1154 [2021](https://doi.org/10.5194/acp-21-773-2021), 2021.
1155
1156 Holloway, T., Levy, H., and Kasibhatla, P.: Global distribution of carbon monoxide, *J. Geophys. Res.*, 105, D10,
1157 12123-12147, doi:10.1029/1999JD901173, 2000.
1158
1159 Horowitz, J.: Italy Locks Down Much of the Country's North Over the Coronavirus,
1160 <https://www.nytimes.com/2020/03/07/world/europe/coronavirus-italy.html>, last access: 17 June 2020, 2020a.
1161
1162 Horowitz, J.: Hope and Worry Mingle as Countries Relax Coronavirus Lockdowns,
1163 <https://www.nytimes.com/2020/05/04/world/europe/coronavirus-restrictions.html>, last access: 17 June 2020, 2020b.
1164
1165 Huang, G. and Sun, K.: Non-negligible impacts of clean air regulations on the reduction of tropospheric NO₂ over
1166 East China during the COVID-19 pandemic observed by OMI and TROPOMI, *Sci. Total Environ.*, 745, 141023,
1167 doi:10.1016/j.scitotenv.2020.141023, 2020.
1168



- 1169 Ialongo, I., Virta, H., Eskes, H., Hovila, J., and Douros, J.: Comparison of TROPOMI/Sentinel-5 Precursor NO₂
1170 observations with ground-based measurements in Helsinki, *Atmos. Meas. Tech.*, 13, 205–218, doi:10.5194/amt-13-
1171 205-2020, 2020.
- 1172
- 1173 Jain, S. and Sharma, T.: Social and travel lockdown impact considering Coronavirus disease (COVID-19) on air
1174 quality in megacities of India: present benefits, future challenges and way forward, *Aerosol Air Qual. Res.*, 20, 1222–
1175 1236, doi:10.4209/aaqr.2020.04.0171, 2020.
- 1176
- 1177 Jennings, R., Philippines allows soft post-lockdown reopening to avert dire economic fall,
1178 [https://www.voanews.com/east-asia-pacific/philippines-allows-soft-post-lockdown-reopening-avert-dire-economic-](https://www.voanews.com/east-asia-pacific/philippines-allows-soft-post-lockdown-reopening-avert-dire-economic-fall)
1179 [fall](https://www.voanews.com/east-asia-pacific/philippines-allows-soft-post-lockdown-reopening-avert-dire-economic-fall), last access: 17 June 2020, 2020.
- 1180
- 1181 Judd, L. M., Al-Saadi, J. A., Szykman, J. J., Valin, L. C., Janz, S. J., Kowalewski, M. G., Eskes, H. J., Veeffkind, J. P.,
1182 Cede, A., Mueller, M., Gebetsberger, M., Swap, R., Pierce, R. B., Nowlan, C. R., Abad, G. G., Nehrir, A., and
1183 Williams, D.: Evaluating Sentinel-5P TROPOMI tropospheric NO₂ column densities with airborne and Pandora
1184 spectrometers near New York City and Long Island Sound, *Atmos. Meas. Tech.*, 13, 6113–6140, doi:10.5194/amt-
1185 13-6113-2020, 2020.
- 1186
- 1187 Kharol, S. K., Fioletov, V., McLinden, C. A., Shephard, M. W., Sioris, C. E., Li, C., and Krotkov, N.A.: Ceramic
1188 industry at Morbi as a large source of SO₂ emissions in India, *Atmos. Environ.*,
1189 223, doi:10.1016/j.atmosenv.2019.117243, 2019.
- 1190
- 1191 Krol, M., Houweling, S., Bregman, B., van den Broek, M., Segers, A., van Velthoven, P., Peters, W., Dentener, F., and
1192 Bergamaschi, P.: The two-way nested global chemistry-transport zoom model TM5: algorithm and applications,
1193 *Atmos. Chem. Phys.*, 5, 417–432, doi:10.5194/acp-5-417-2005, 2005.
- 1194
- 1195 Kroll, J. H., Heald, C. L., Cappa, C. D., Farmer, D. K., Fry, J. L., Murphy, J. G., and Steiner, A. L.: The complex
1196 chemical effects of COVID-19 shutdowns on air quality, *Nat. Chem.*, 12, 777–779, doi:10.1038/s41557-020-0535-z,
1197 2020.
- 1198
- 1199 Kumari, P., and Toshniwal, D.: Impact of lockdown measures during COVID-19 on air quality—a case study of India.
1200 *Int. J. Environ. Heal. R.*, 1-8, doi:10.1080/09603123.2020.1778646, 2020.
- 1201
- 1202 Lambert, J.-C., S. Compernelle, K.-U. Eichmann, M. de Graaf, D. Hubert, A. Keppens, Q. Kleipool, B. Langerock,
1203 M.K. Sha, T. Verhoelst, T. Wagner, C. Ahn, A. Argyrouli, D. Balis, K.L. Chan, I. De Smedt, H. Eskes, A.M. Fjæraa,
1204 K. Garane, J.F. Gleason, F. Goutail, J. Granville, P. Hedelt, K.-P. Heue, G. Jaross, M.L. Koukoulis, J. Landgraf, R.
1205 Lutz, S. Nanda, S. Niemeijer, A. Pazmiño, G. Pinaridi, J.-P. Pommereau, A. Richter, N. Rozemeijer, M. Sneep, D.



- 1206 Stein Zweers, N. Theys, G. Tilstra, O. Torres, P. Valks, J. van Geffen, C. Vigouroux, P. Wang, and M. Weber. S5P
1207 MPC Routine Operations Consolidated Validation Report series, Issue #09, document number: S5P-MPC-IASB-
1208 ROCVR-09.01.01-20201221, 9.01.01, Royal Belgian Institute for Space Aeronomy, Brussels, Belgium, [http://mpc-
1210 vdaf.tropomi.eu/index.php?option=com_vdaf&view=showReport&format=rawhtml&id=45](http://mpc-
1209 vdaf.tropomi.eu/index.php?option=com_vdaf&view=showReport&format=rawhtml&id=45)
1211 2020.
- 1212 Landgraf, J., aan de Brugh, J., Scheepmaker, R., Borsdorff, T., Hu, H., Houweling, S., Butz, A., Aben, I., and
1213 Hasekamp, O.: Carbon monoxide total column retrievals from TROPOMI shortwave infrared measurements, Atmos.
1214 Meas. Tech., 9, 4955–4975, doi:10.5194/amt-9-4955-2016, 2016.
- 1215
- 1216 Landgraf, J., aan de Brugh, J., Scheepmaker, R. A., Borsdorff, T., Houweling, S., and Hasekamp, O. P.: Algorithm
1217 Theoretical Baseline Document for Sentinel-5 Precursor: Carbon Monoxide Total Column Retrieval, document
1218 number: SRON-S5P-LEV2-RP-002, 1.10, SRON Netherlands Institute for Space Research, Utrecht, The Netherlands,
1219 <https://sentinels.copernicus.eu/web/sentinel/technical-guides/sentinel-5p/products-algorithms>, 2018.
- 1220
- 1221 Landgraf, J., Borsdorff, T., Langerock, B., and Keppens, A.: S5P Mission Performance Centre Carbon Monoxide
1222 [L2_CO___] Readme, document number: S5P-MPC-SRON-PRF-CO, 1.5, SRON Netherlands Institute for Space
1223 Research, Utrecht, The Netherlands, [https://sentinels.copernicus.eu/web/sentinel/technical-guides/sentinel-
1225 5p/products-algorithms](https://sentinels.copernicus.eu/web/sentinel/technical-guides/sentinel-
1224 5p/products-algorithms), 2020.
- 1226 Lee, C., Martin, R. V., van Donkelaar, A., Lee, H., Dickerson, R. R., Hains, J. C., Krotkov, N., Richter, A., Vinnikov,
1227 K., and Schwab, J. J.: SO₂ emissions and lifetimes: Estimates from inverse modeling using in situ and global, space-
1228 based (SCIAMACHY and OMI) observations, J. Geophys. Res., 116, D06304, doi:10.1029/2010JD014758, 2011.
- 1229
- 1230 Lee, J. D., Drysdale, W. S., Finch, D. P., Wilde, S. E., and Palmer, P. I.: UK surface NO₂ levels dropped by 42%
1231 during the COVID-19 lockdown: impact on surface O₃, Atmos. Chem. Phys., doi:10.5194/acp-2020-838, 2020.
- 1232
- 1233 Le Quéré, C., Jackson, R. B., Jones, M. W., Smith, A. J. P., Abernethy, S., Andrew, R. M., De-Gol, A. J., Willis, D.
1234 R., Shan, Y., Canadell, J. G., Friedlingstein, P., Creutzig F., and Peters, G. P.: Temporary reduction in daily global
1235 CO₂ emisisions during the COVID-19 forced confinement, Nat. Clim. Chang., 10, 647-653, doi:10.1038/s41558-020-
1236 0797-x, 2020.
- 1237
- 1238 Lerot, C., Stavrakou, T., De Smedt, I., Müller, J.-F., and Van Roozendaal, M.: Glyoxal vertical 576 columns from
1239 GOME-2 backscattered light measurements and comparisons with a global 577 model. Atmos. Chem. Phys., 10,
1240 12059-12072, 2010.
- 1241



- 1242 Lerot, C., Stavrakou, T., Van Roozendael, M., Alvarado, L. M. A., and Richter, A.: GLYoxal Retrievals from
1243 TROPOMI (GLYRETRO) ATBD, S5p+Innovation – theme 1 (CHOCHO), 5p+I_CHOCHO_BIRA_ATBD, issue
1244 2.1, 16 November 2020, <https://glyretro.aeronomie.be/>, 2020.
- 1245
- 1246 Leung, K., Wu, J. Liu, D., and Leung, G. M.: First-wave COVID-19 transmissibility and severity in China outside
1247 Hubei after control measures, and second-wave scenario planning: a modelling impact assessment, *The Lancet*, 395
1248 (10233), 1382-1393, [doi:10.1016/S0140-6736\(20\)30746-7](https://doi.org/10.1016/S0140-6736(20)30746-7), 2020.
- 1249
- 1250 Li, C., McLinden, C., Fioletov, V., Krotkov, N., Carn, S., Joiner, J., Streets, D., He, H., Ren, X., Zhanqing Li, Z., and
1251 Dickerson, R. R.: India Is Overtaking China as the World’s Largest Emitter of Anthropogenic Sulfur Dioxide, *Sci.*
1252 *Rep.*, 7, 14304, [doi:10.1038/s41598-017-14639-8](https://doi.org/10.1038/s41598-017-14639-8), 2017.
- 1253
- 1254 Liu, F., Page, A., Strode, S. A., Yoshida, Y., Choi, S., Zheng, B., Lamsal, L. N., Li, C., Krotkov, N. A., Eskes, H.,
1255 van der A, R., Veefkind, P., Levelt, P. F., Hauser, O. P., and Joiner, J.: Abrupt decline in tropospheric nitrogen dioxide
1256 over China after the outbreak of COVID-19, *Sci. Adv.*, 6, 28, eabc2992, [doi:10.1126/sciadv.abc2992](https://doi.org/10.1126/sciadv.abc2992), 2020.
- 1257
- 1258 Lorente, A., Boersma, K. F., Eskes, H. J., Veefkind, J. P., van Geffen, J. H. G. M., de Zeeuw, M. B., Denier van der
1259 Gon, H. A. C., Beirle, S., and Krol, M. C.: Quantification of nitrogen oxides emissions from build-up of pollution over
1260 Paris with TROPOMI, *Sci. Rep.*, 9, 20033, [doi:10.1038/s41598-019-56428-5](https://doi.org/10.1038/s41598-019-56428-5), 2019.
- 1261
- 1262 Loyola, D. G., Gimeno García, S., Lutz, R., Argyrouli, A., Romahn, F., Spurr, R. J. D., Pedernana, M., Doicu, A.,
1263 Molina García, V., and Schüssler, O.: The operational cloud retrieval algorithms from TROPOMI on board Sentinel-
1264 5 Precursor, *Atmos. Meas. Tech.*, 11, 409–427, [doi:10.5194/amt-11-409-2018](https://doi.org/10.5194/amt-11-409-2018), 2018.
- 1265
- 1266 Ludewig, A., Kleipool, Q., Bartstra, R., Landzaat, R., Leloux, J., Loots, E., Meijering, P., van der Plas, E., Rozemeijer,
1267 N., Vonk, F., and Veefkind, P.: In-flight calibration results of the TROPOMI payload on board the Sentinel-5
1268 Precursor satellite, *Atmos. Meas. Tech.*, 13, 3561–3580, [doi:10.5194/amt-13-3561-2020](https://doi.org/10.5194/amt-13-3561-2020), 2020.
- 1269
- 1270 Mahato, S., Pal, S., and Ghosh, K. G.: Effect of lockdown amid COVID-19 pandemic on air quality of the megacity
1271 Delhi, India, *Sci. Total Environ.*, 730, 139086, [doi:10.1016/j.scitotenv.2020.139086](https://doi.org/10.1016/j.scitotenv.2020.139086), 2020.
- 1272
- 1273 Makooi, B.: Key points of France’s strategy for lifting its nationwide Covid-19 lockdown.
1274 [https://www.france24.com/en/20200429-key-points-of-france-s-strategy-for-lifting-its-nationwide-covid-19-](https://www.france24.com/en/20200429-key-points-of-france-s-strategy-for-lifting-its-nationwide-covid-19-lockdown)
1275 [lockdown](https://www.france24.com/en/20200429-key-points-of-france-s-strategy-for-lifting-its-nationwide-covid-19-lockdown), last access: 17 June 2020, 2020.
- 1276



- 1277 Masaki, T., Nakamura, S., Newhouse, D.: How is the COVID-19 crisis affecting nitrogen dioxide emissions in Sub-
1278 Saharan Africa? Poverty and Equity Notes, No. 21. World Bank, Washington, DC, World Bank.
1279 <https://openknowledge.worldbank.org/handle/10986/33801>, License: CC BY 3.0 IGO, 2020.
1280
- 1281 Matthews, A.: Coronavirus: 5 things New Zealand got right, Deutsche Welle, <https://p.dw.com/p/3dSVh>, last access:
1282 2 July 2020, 2020.
1283
- 1284 Mbah, F.: Businesses reopen as Nigeria eases coronavirus lockdown. Available from
1285 [https://www.aljazeera.com/news/2020/05/businesses-reopen-nigeria-eases-coronavirus-lockdown-](https://www.aljazeera.com/news/2020/05/businesses-reopen-nigeria-eases-coronavirus-lockdown-200504094440082.html)
1286 [200504094440082.html](https://www.aljazeera.com/news/2020/05/businesses-reopen-nigeria-eases-coronavirus-lockdown-200504094440082.html), last access: 17 June 2020, 2020.
1287
- 1288 Menon, P.: ‘Stay at home’ New Zealand PM urges ahead of coronavirus lockdown. Available from
1289 [https://www.reuters.com/article/us-health-coronavirus-newzealand/stay-at-home-new-zealand-pm-urges-ahead-of-](https://www.reuters.com/article/us-health-coronavirus-newzealand/stay-at-home-new-zealand-pm-urges-ahead-of-coronavirus-lockdown-idUSKBN21A3RN)
1290 [coronavirus-lockdown-idUSKBN21A3RN](https://www.reuters.com/article/us-health-coronavirus-newzealand/stay-at-home-new-zealand-pm-urges-ahead-of-coronavirus-lockdown-idUSKBN21A3RN), last access: 17 June 2020, 2020.
1291
- 1292 Millet, D. B., Jacob, D. J., Boersma, K. F., Fu, T. M., Kurosu, T. P., Chance, K., Heald, C. L., and Guenther, A.:
1293 Spatial distribution of isoprene emissions from North America derived from formaldehyde column measurements by
1294 the OMI satellite sensor, *J. Geophys. Res.*, 113, D02307, doi:10.1029/2007jd008950, 2008.
1295
- 1296 Minder, R. and Peltier, E.: Spain imposes nationwide lockdown to fight coronavirus. Available from
1297 <https://www.nytimes.com/2020/03/14/world/europe/spain-coronavirus.html>, last access: 17 June 2020, 2020.
1298
- 1299 Misculin N., and Garrison C.: Argentina extends lockdown in Buenos Aires as coronavirus cases surpass 20,000.
1300 Available from [https://www.thejakartapost.com/news/2020/06/05/argentina-extends-lockdown-in-buenos-aires-as-](https://www.thejakartapost.com/news/2020/06/05/argentina-extends-lockdown-in-buenos-aires-as-coronavirus-cases-surpass-20000.html)
1301 [coronavirus-cases-surpass-20000.html](https://www.thejakartapost.com/news/2020/06/05/argentina-extends-lockdown-in-buenos-aires-as-coronavirus-cases-surpass-20000.html), last access: 17 June 2020, 2020.
1302
- 1303 Miyazaki, K., Bowman, K., Sekiya, T., Jiang, Z., Chen, X., Eskes, H., Ru, M., Zhang, Y., and Shindell, D.: Air
1304 quality response in China linked to the 2019 novel coronavirus (COVID-19) lockdown, *Geophys. Res. Lett.*, 47,
1305 e2020GL089252, doi:10.1029/2020GL089252, 2020.
1306
- 1307 Müller, J.-F., Stavrou, T., Bauwens, M., Compornolle, S., and Peeters, J.: Chemistry and deposition in the Model
1308 of Atmospheric composition at Global and Regional scales using Inversion Techniques for Trace gas Emissions
1309 (MAGRITTE v1.0). Part B. Dry deposition, *Geosci. Model Dev. Discuss.*, 1–49, doi:10.5194/gmd-2018-317, 2018.
1310
- 1311 Müller, J.-F., Stavrou, T., and Peeters, J.: Chemistry and deposition in the Model of Atmospheric composition at
1312 Global and Regional scales using Inversion Techniques for Trace gas Emissions (MAGRITTE v1.1) – Part 1:
1313 Chemical mechanism, *Geosci. Model Dev.*, 12, 2307–2356, doi:10.5194/gmd-12-2307-2019, 2019.



1314
1315 Muñoz Sabater, J.: ERA5-Land monthly averaged data from 1981 to present, Copernicus Climate Change Service
1316 (C3S) Climate Data Store (CDS) [data set], last access: 09 June 2021, doi:10.24381/cds.68d2bb30, 2019a.
1317
1318 Muñoz Sabater, J.: ERA5-Land hourly averaged data from 1981 to present, Copernicus Climate Change Service (C3S)
1319 Climate Data Store (CDS) [data set], last access: 09 June 2021, doi:10.24381/cds.e2161bac, 2019b.
1320
1321 New South Wales Public Health: Public Health (COVID-19 Restrictions on Gathering and Movement) Order 2020,
1322 <https://www.legislation.nsw.gov.au>, last access: 2 July 2020, 2020.
1323
1324 Odunsi, P.: Africa: COVID-19 deaths hits 37,000, Nigeria on top 5, Daily Post Nigeria,
1325 <https://dailypost.ng/2020/10/06/africa-covid-19-deaths-hits-37000-nigeria-on-top-5/>, last access: 30 March 2021,
1326 2020.
1327
1328 Onishi, N. and Méheut, C.: Paris, a magnet for the world, becomes a ghost city after a lockdown takes effect. Available
1329 from <https://www.nytimes.com/2020/03/17/world/europe/paris-coronavirus-lockdown.html>, last access: 17 June
1330 2020, 2020.
1331
1332 Orjinmo, N.: Coronavirus lockdown: Nigerians cautious as restrictions eased in Lagos and Abuja. Available from
1333 <https://www.bbc.com/news/world-52526923>, last access: 17 June 2020, 2020.
1334
1335 Palmer, P. I., Jacob, D. J., Chance, K., Martin, R. V., Spurr, R. J. D., Kurosu, T. P., Bey, I., Yantosca, R., Fiore, A.,
1336 and Li, Q.: Air mass factor formulation for spectroscopic measurements from satellites: Application to formaldehyde
1337 retrievals from the Global Ozone Monitoring Experiment, *J. Geophys. Res. Atmos.*, 106, D13, 14539–14550,
1338 doi:10.1029/2000JD900772, 2001.
1339
1340 Pasley, J.: Mexico has moved to 'Phase 3' — its most serious level of coronavirus alert — and faces a looming
1341 outbreak. Here's how it got to this point, [https://www.insider.com/photo-mexico-coronavirus-move-to-phase-three-](https://www.insider.com/photo-mexico-coronavirus-move-to-phase-three-2020-4)
1342 [2020-4](https://www.insider.com/photo-mexico-coronavirus-move-to-phase-three-2020-4), last access: 17 June 2020, 2020.
1343
1344 Patel S.: When Is California Reopening? The New York Times. Available from
1345 <https://www.nytimes.com/article/coronavirus-california-reopening-phases.html>, last access: 17 June 2020, 2020.
1346
1347 POSOCO, Power System Operation Corporation Limited, National Load Despatch Centre: [https://posoco.in/covid-](https://posoco.in/covid-19/)
1348 [19/](https://posoco.in/covid-19/), last access: 30 March 2021.
1349



- 1350 Prabhjote, G.: The most congested cities in India low lie vacant midst the nationwide lockdown, Business Insider
1351 India, [https://www.businessinsider.in/india/news/most-congested-cities-in-india-low-lie-vacant-midst-the-](https://www.businessinsider.in/india/news/most-congested-cities-in-india-low-lie-vacant-midst-the-nationwide-lockdown/articleshow/75243376.cms)
1352 [nationwide-lockdown/articleshow/75243376.cms](https://www.businessinsider.in/india/news/most-congested-cities-in-india-low-lie-vacant-midst-the-nationwide-lockdown/articleshow/75243376.cms), last access: 30 March 2021, 2020.
- 1353
- 1354 Raszewski, E., and Garrison, C.: Buenos Aires lockdown extended until June 7 after rise in coronavirus cases, Reuters,
1355 [https://www.reuters.com/article/us-health-coronavirus-argentina/buenos-aires-lockdown-extended-until-june-7-](https://www.reuters.com/article/us-health-coronavirus-argentina/buenos-aires-lockdown-extended-until-june-7-after-rise-in-coronavirus-cases-idUSKBN22Z0YB?il=0)
1356 [after-rise-in-coronavirus-cases-idUSKBN22Z0YB?il=0](https://www.reuters.com/article/us-health-coronavirus-argentina/buenos-aires-lockdown-extended-until-june-7-after-rise-in-coronavirus-cases-idUSKBN22Z0YB?il=0), last access: 17 June 2020, 2020.
- 1357
- 1358 Romahn, F., Pedernana, M., Loyola, D., Apituley, A., Sneep, M., Veeffkind, J. P., De Smedt, I., and Chan, K. L.:
1359 Sentinel-5 precursor/TROPOMI Level 2 Product User Manual Formaldehyde HCHO, document number: S5P-L2-
1360 DLR-PUM-400F, 2.01.00, DLR, German Aerospace Center, Oberpfaffenhofen, Germany,
1361 <https://sentinels.copernicus.eu/web/sentinel/technical-guides/sentinel-5p/products-algorithms>, 2020.
- 1362
- 1363 Saleh, I.: Iraq locks down 6 districts in Baghdad to stem virus. Available from [https://www.aa.com.tr/en/latest-on-](https://www.aa.com.tr/en/latest-on-coronavirus-outbreak/iraq-locks-down-6-districts-in-baghdad-to-stem-virus/1845104)
1364 [coronavirus-outbreak/iraq-locks-down-6-districts-in-baghdad-to-stem-virus/1845104](https://www.aa.com.tr/en/latest-on-coronavirus-outbreak/iraq-locks-down-6-districts-in-baghdad-to-stem-virus/1845104), last access: 17 June 2020,
1365 2020.
- 1366
- 1367 Shi, X. and Brasseur, G. P.: The response in air quality to the reduction of Chinese economic activities during the
1368 COVID-19 outbreak, Geophys. Res. Lett., 47, e2020GL088070, doi:10.1029/2020GL088070, 2020.
- 1369
- 1370 Singh, K. D., Goel, V., Kumar, H., and Gettleman, J.: India, Day 1: World's Largest Coronavirus Lockdown Begins,
1371 The New York Times, <https://www.nytimes.com/2020/03/25/world/asia/india-lockdown-coronavirus.html>, last
1372 access: 30 March 2021, 2020.
- 1373
- 1374 Sonali P.: Australia's biggest state to ease coronavirus lockdown from May 15, [https://www.reuters.com/article/us-](https://www.reuters.com/article/us-health-coronavirus-australia/australias-biggest-state-to-ease-coronavirus-lockdown-from-may-15-idUSKBN22M01U)
1375 [health-coronavirus-australia/australias-biggest-state-to-ease-coronavirus-lockdown-from-may-15-](https://www.reuters.com/article/us-health-coronavirus-australia/australias-biggest-state-to-ease-coronavirus-lockdown-from-may-15-idUSKBN22M01U)
1376 [idUSKBN22M01U](https://www.reuters.com/article/us-health-coronavirus-australia/australias-biggest-state-to-ease-coronavirus-lockdown-from-may-15-idUSKBN22M01U), last access: 17 June 2020, 2020.
- 1377
- 1378 Spurr R., and Christi M.: The LIDORT and VLIDORT Linearized Scalar and Vector Discrete Ordinate Radiative
1379 Transfer Models: Updates in the Last 10 Years. In: Kokhanovsky A. (eds) Springer Series in Light Scattering. Springer
1380 Series in Light Scattering. Springer, Cham., doi:10.1007/978-3-030-03445-0_1, 2019.
- 1381
- 1382 Stavrakou, T., Müller, J.-F., De Smedt, I., Van Roozendael, M., Kanakidou, M., Vrekoussis, M., Wittrock, F., Richter,
1383 A., and Burrows, J. P.: The continental source of glyoxal estimated by the synergistic use of spaceborne measurements
1384 and inverse modelling, Atmos. Chem. Phys., 9, 8431–8446, doi:10.5194/acp-9-8431-2009, 2009.
- 1385



- 1386 Stavrakou, T., Müller, J.-F., Bauwens, M., De Smedt, I., Van Roozendael, M., and Guenther, A. B.: Impact of short-
1387 term climate variability on volatile organic compounds emissions assessed using OMI satellite formaldehyde
1388 observations. *Geophys. Res. Lett.*, 45, 8681–8689, doi:10.1029/2018GL078676, 2018.
- 1389
- 1390 Sun, W., Zhu, L., De Smedt, I., Bai, B., Pu, D., Chen, Y., Shu, L., Wang, D., Fu, T.-M., Wang, X., and Yang, X.:
1391 Global significant changes in formaldehyde (HCHO) columns observed from space at the early stage of the COVID-
1392 19 pandemic, *Geophys. Res. Lett.*, 48, e2020GL091265, doi:10.1029/2020GL091265, 2021.
- 1393
- 1394 Tack, F., Merlaud, A., Iordache, M.-D., Pinardi, G., Dimitropoulou, E., Eskes, H., Bomans, B., Veeffkind, P., and Van
1395 Roozendael, M.: Assessment of the TROPOMI tropospheric NO₂ product based on airborne APEX observations,
1396 *Atmos. Meas. Tech.*, 14, 615–646, doi:10.5194/amt-14-615-2021, 2021.
- 1397
- 1398 Tan, P. H., Chou, C., Liang, J. Y., Chou, C. C. K., and Shiu, C. J.: Air pollution “holiday effect” resulting from the
1399 Chinese New Year, *Atmos. Environ.*, 43(13), 2114–2124, doi:10.1016/j.atmosenv.2009.01.037, 2009.
- 1400
- 1401 The Star: Iraq on total lockdown until March 28 over virus fears,
1402 <https://www.thestar.com.my/news/regional/2020/03/22/iraq-on-total-lockdown-until-march-28-over-virus-fears>, last
1403 access: 17 June 2020, 2020.
- 1404
- 1405 Theys, N., Fioletov, V., Li, C., De Smedt, I., Lerot, C., McLinden, C., Krotkov, N., Griffin, D., Clarisse, L., Hedelt,
1406 P., Loyola, D., Wagner, T., Kumar, V., Innes, A., Ribas, R., Hendrick, F., Vlietinck, J., Brenot, H., and Van
1407 Roozendael, M.: A Sulfur Dioxide Covariance-Based Retrieval Algorithm (COBRA): application to TROPOMI
1408 reveals new emission sources, *Atmos. Chem. Phys. Discuss.* [preprint], doi:10.5194/acp-2021-294, in review, 2021.
- 1409
- 1410 Uchoa, P.: Brazil coronavirus: 'Our biggest problem is fake news', BBC, <https://www.bbc.com/news/world-latin-america-52739734>, last access: 17 June 2020, 2020.
- 1411
- 1412
- 1413 Veeffkind, J. P., Aben, I., McMullan, K., Forster, H., de Vries, J., Otter, G., Claas, J., Eskes, H. J., de Haan, J. F.,
1414 Kleipool, Q., van Weele, M., Hasekamp, O., Hoogeveen, R., Landgraf, J., Snel, R., Tol, P., Ingmann, P., Voors, R.,
1415 Kruizinge, B., Vink, R., Visser, H., and Levelt, P. F.: TROPOMI on the ESA Sentinel-5 Precursor: A GMES mission
1416 for global observations of the atmospheric composition for climate, air quality and ozone layer applications, *Remote
1417 Sens. Environ.*, 120, 70–83, 2012.
- 1418
- 1419 Verhoelst, T., Compennolle, S., Pinardi, G., Lambert, J.-C., Eskes, H. J., Eichmann, K.-U., Fjæraa, A. M., Granville,
1420 J., Niemeijer, S., Cede, A., Tiefengraber, M., Hendrick, F., Pazmiño, A., Bais, A., Bazureau, A., Boersma, K. F.,
1421 Bogner, K., Dehn, A., Donner, S., Elokhov, A., Gebetsberger, M., Goutail, F., Grutter de la Mora, M., Gruzdev, A.,
1422 Gratsea, M., Hansen, G. H., Irie, H., Jepsen, N., Kanaya, Y., Karagkiozidis, D., Kivi, R., Kreher, K., Levelt, P. F.,



- 1423 Liu, C., Müller, M., Navarro Comas, M., PETERS, A. J. M., Pommereau, J.-P., Portafaix, T., Prados-Roman, C.,
1424 Puentedura, O., Querel, R., Remmers, J., Richter, A., Rimmer, J., Rivera Cárdenas, C., Saavedra de Miguel, L.,
1425 Sinyakov, V. P., Stremme, W., Strong, K., Van Roozendaal, M., Veefkind, J. P., Wagner, T., Wittrock, F., Yela
1426 González, M., and Zehner, C.: Ground-based validation of the Copernicus Sentinel-5P TROPOMI NO₂ measurements
1427 with the NDACC ZSL-DOAS, MAX-DOAS and Pandonia global networks, *Atmos. Meas. Tech.*, 14, 481–510,
1428 doi:10.5194/amt-14-481-2021, 2021.
- 1429
- 1430 Vigouroux, C., Langerock, B., Bauer Aquino, C. A., Blumenstock, T., Cheng, Z., De Mazière, M., De Smedt, I.,
1431 Grutter, M., Hannigan, J. W., Jones, N., Kivi, R., Loyola, D., Lutsch, E., Mahieu, E., Makarova, M., Metzger, J.-M.,
1432 Morino, I., Murata, I., Nagahama, T., Notholt, J., Ortega, I., Palm, M., Pinardi, G., Röhlings, A., Smale, D., Stremme,
1433 W., Strong, K., Sussmann, R., Té, Y., van Roozendaal, M., Wang, P., and Winkler, H.: TROPOMI–Sentinel-5
1434 Precursor formaldehyde validation using an extensive network of ground-based Fourier-transform infrared stations,
1435 *Atmos. Meas. Tech.*, 13, 3751–3767, doi:10.5194/amt-13-3751-2020, 2020.
- 1436
- 1437 Wahlquist, C.: Australia's coronavirus lockdown – the first 50 days,
1438 <https://www.theguardian.com/world/2020/may/02/australias-coronavirus-lockdown-the-first-50-days>, last access: 17
1439 June 2020, 2020.
- 1440 Wang, Y., Yuan, Y., Wang, Q., Liu, C. G., Zhi, Q., and Cao, J.: Changes in air quality related to the control of
1441 coronavirus in China: Implications for traffic and industrial emissions, *Sci. Total Environ.*, 731, 139133,
1442 doi:10.1016/j.scitotenv.2020.139133, 2020.
- 1443
- 1444 Wang, Z., Zheng, F., Zhang, W., and Wang, S.: Analysis of SO₂ Pollution Changes of Beijing-Tianjin-Hebei Region
1445 over China Based on OMI Observations from 2006 to 2017, *Adv. Meteorol.*, 2018, doi:10.1155/2018/8746068, 2018.
- 1446
- 1447 Williams, J. E., Boersma, K. F., Le Sager, P., and Verstraeten, W. W.: The high-resolution version of TM5-MP for
1448 optimized satellite retrievals: description and validation, *Geosci. Model Dev.*, 10, 721–750, doi:10.5194/gmd-10-721-
1449 2017, 2017.
- 1450 Winter, S.: Ramaphosa announces 21 day coronavirus lockdown for South Africa,
1451 [https://businesstech.co.za/news/government/383927/ramaphosa-announces-21-day-coronavirus-lockdown-for-south-](https://businesstech.co.za/news/government/383927/ramaphosa-announces-21-day-coronavirus-lockdown-for-south-africa/)
1452 [africa/](https://businesstech.co.za/news/government/383927/ramaphosa-announces-21-day-coronavirus-lockdown-for-south-africa/), last access: 17 June 2020, 2020.
- 1453
- 1454 Zhang, R., Zhang, Y., Lin, H., Feng, X., Fu, T.-M., and Wang, Y.: NO_x Emission Reduction and Recovery during
1455 COVID-19 in East China, *Atmosphere (Basel)*, 11(4), 433, doi:10.3390/atmos11040433, 2020.
- 1456
- 1457 Zhang, Z., Arshad, A., Zhang, C., Hussain, S. and Li, W.: Unprecedented Temporary Reduction in Global Air
1458 Pollution Associated with COVID-19 Forced Confinement: A Continental and City Scale Analysis, *Remote Sens.*,
1459 12(15), 2420, doi:10.3390/rs12152420, 2020.



- 1460
- 1461 Zhao, N., G. Wang, G. Li, J. Lang and H. Zhang: Air pollution episodes during the COVID-19 outbreak in the Beijing–
1462 Tianjin–Hebei region of China: An insight into the transport pathways and source distribution. *Environmental*
1463 *Pollution* 267, 115617, <https://doi.org/10.1016/j.envpol.2020.115617>, 2020.
- 1464
- 1465 Zhao, Y., Zhang, K., Xu, X., Shen, H., Zhu, X., Zhang, Y., Hu, Y. and Shen, G.: Substantial Changes in Nitrogen
1466 Dioxide and Ozone after Excluding Meteorological Impacts during the COVID-19 Outbreak in Mainland China,
1467 *Environ. Sci. Technol. Lett.*, 7(6), 402–408, doi:10.1021/acs.estlett.0c00304, 2020.
- 1468
- 1469 Zheng, B., Tong, D., Li, M., Liu, F., Hong, C., Geng, G., Li, H., Li, X., Peng, L., Qi, J., Yan, L., Zhang, Y., Zhao, H.,
1470 Zheng, Y., He, K., and Zhang, Q.: Trends in China’s anthropogenic emissions since 2010 as the consequence of clean
1471 air actions, *Atmos. Chem. Phys.*, 18(19), 14095–14111, doi:10.5194/acp-18-14095-2018, 2018a.
- 1472
- 1473 Zheng, B., Chevallier, F., Ciais, P., Yin, Y., Deeter, M. N., Worden, H. M., Wang, Y., Zhang, Q., and He, K.: Rapid
1474 decline in carbon monoxide emissions and export from East Asia between years 2005 and 2016, *Environ. Res. Lett.*,
1475 13(4), doi:10.1088/1748-9326/aab2b3, 2018b.
- 1476
- 1477 Zhu, L., Mickley, L. J., Jacob, D. J., Marais, E. A., Sheng, J., Hu, L., Abad, G. G., and Chance, K.: Long-term (2005–
1478 2014) trends in formaldehyde (HCHO) columns across North Americas seen by the OMI satellite instrument:
1479 Evidence of changing emissions of volatile organic compounds, *Geophys. Res. Lett.*, 44, 7079–7086,
1480 doi:10.1002/2017GL073859, 2017.